Shahrood University of Technology

Journal of Mining and Environment (JME)

Journal homepage: www.jme.shahroodut.ac.ir

Iranian Society of Mining Engineering (IRSME)

# A Geospatial Approach to Landslide Susceptibility Mapping of Spiti, India

Devraj Dhakal* and Kanwarpreet Singh

*Department of Civil Engineering, Chandigarh University, Mohali, India*

***Article Info***

*Received 19 June 2024*

*Received in Revised form 25 July 2024*

*Accepted 10 August 2024*

*Published online 10 August 2024*

*DOI: 10.22044/jme.2024.14684.2779*

***Keywords***

*Landslide Susceptibility Mapping (LSM)*

*Frequency Ratio (FR)*

*Information Value (IV)*

*Geospatial Analysis*

*Landslide Density Index (LDI)*

***Abstract***

Landslides pose significant risks to human life, infrastructure, and the environment, particularly in geologically unstable regions like the Himalayas. This study aims to develop and validate landslide susceptibility maps using Frequency Ratio (FR) and Information Value (IV) models within a GIS framework. Employing high-resolution geospatial data, including geomorphological, topographical, and hydrological factors derived from high-resolution digital elevation models (DEMs) and other geospatial datasets. The susceptibility maps were classified into five categories: Low, Moderate, High, Very High, and Extremely High. The models were trained and validated using a landslide inventory of 1313 landslide events, with a 70:30 split for training and testing datasets. The predictive performance of the models was evaluated using the Area Under the Curve (AUC) of the Receiver Operating Characteristic (ROC) curve, yielding AUC values of 84.1 for the FR model and 83.9 for the IV model. The Landslide Density Index (LDI) further confirmed the models' reliability, indicating higher landslide densities in the predicted high-susceptibility zones. The study demonstrates that both FR and IV models are effective tools for landslide susceptibility mapping and its validation. The findings highlight the FR model's superior predictive accuracy in this specific area. Future research should leverage advanced machine learning techniques, such as XGBoost, Random Forest (RF), Naive Bayes (NB), and K-Nearest Neighbors (KNN), to enhance the reliability and precision of landslide susceptibility models.

## 1. Introduction

Landslides are a prevalent natural hazard, causing significant damage to life, property, and the environment globally [1–5]. This geohazard is particularly severe in mountainous regions, where steep slopes, heavy rainfall, and geological factors combine to create unstable conditions [6–11]. Landslides occur due to a variety of triggers including intense rainfall, rapid snowmelt, earthquakes, volcanic activity, and human activities such as deforestation and construction [1]. These factors lead to the destabilization of slopes, causing soil, rock, and debris to move downslope rapidly [12].

India is among the most landslide-prone nations in Asia, trailing only China. In the period from 2020 to 2021, India registered some of the highest figures for fatalities caused by landslides globally [13]. Historical events underscore the devastating impact of landslides in the country. For instance, Guwahati, Assam, experienced a catastrophic landslip on September 18, 1948, triggered by heavy rainfall, which claimed the lives of 500 people and buried an entire community. Similarly, Darjeeling, West Bengal, was struck by a disastrous landslip on October 4, 1968, during severe flooding, resulting in over 1000 fatalities and severe disruption of transportation infrastructure. More recently, the Kedarnath landslide in Uttarakhand on July 16, 2013, caused by heavy rainfall and subsequent floods, led to approximately 5700 fatalities and impacted 4200 villages. These incidents highlight the destructive nature of landslides in India, resulting in significant loss of life and extensive damage to infrastructure. Please refer to Figure 2 for a chronological overview of major landslide incidents in India, including the causes and impacts of each event from 1948 to 2020.

✉ *Corresponding author: fewdrd@gmail.com (D. Dhakal)*

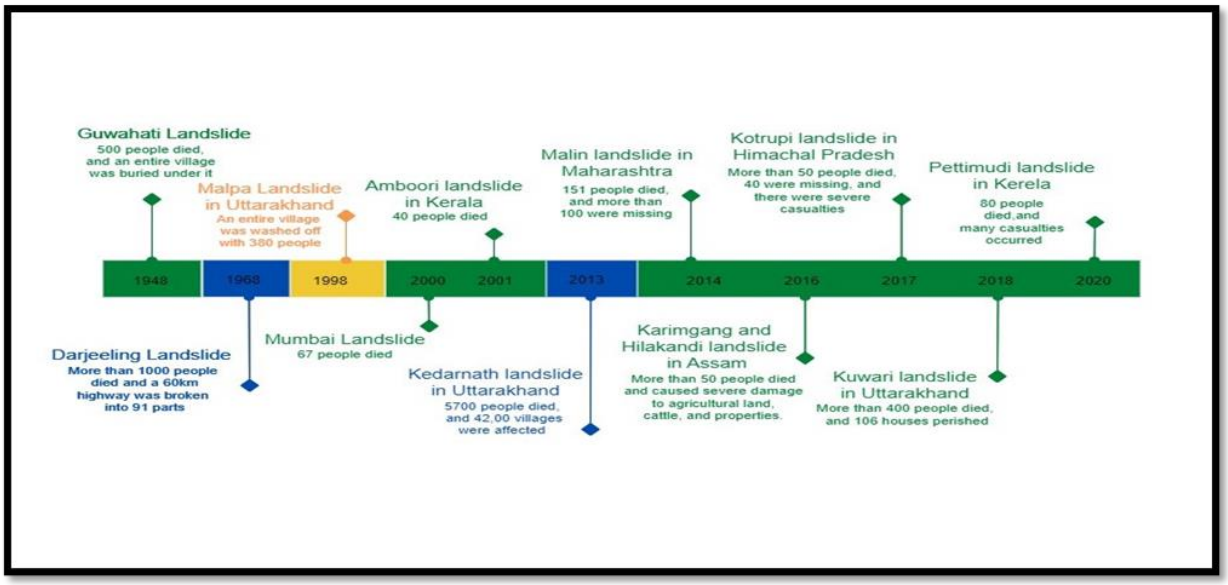


**Figure 1. A major landslide occurred in India.**

Himachal Pradesh, located in the Western Himalayas, frequently experiences landslides due to its complex geological structure, high seismicity, and heavy monsoon rains [12]. Among the various regions in Himachal Pradesh, Spiti Valley stands out due to its unique geographical and climatic conditions, making it a critical area for landslide susceptibility studies. The Spiti Valley is situated between the Kunzum range in the northwest and Khab on the Sutlej River in Kinnaur in the southeast. The Spiti River, originating from the base of the 6,118 m K-111 peak, flows through a catchment area of about 6,300 km². Due to its location in the rain shadow of the main Himalayan range, Spiti does not benefit from the Southwest monsoon and relies on glacier melting for peak river discharge in late summers. The Spiti Valley's unique landscape, featuring steep mountains, deep gorges, and a mix of braided and incised river channels, highlights the need for effective landslide susceptibility zonation (LSZ). The valley's geological features, such as ancient sedimentary deposits and neotectonic activity, further contribute to its landslide risk. Additionally, the sparse vegetation and high-altitude desert environment make the valley particularly vulnerable to landslides. Effective LSZ in Spiti Valley is essential for disaster preparedness, risk mitigation, and sustainable development, given the valley's remoteness and limited infrastructure.

Landslide susceptibility and risk assessment are critical research areas in India, particularly in the Himalayan region spanning Jammu and Kashmir, Himachal Pradesh, Uttarakhand, Sikkim, and Arunachal Pradesh [5,14–17]. These areas are highly susceptible to landslides due to their young geological formations, steep slopes, and heavy monsoon rains, compounded by the impacts of climate change and human activities [13]. The Information Value (IV) [2,3,16,18] and Frequency Ratio (FR) [2,19–22] techniques have been widely applied across various parts of the Indian Himalayas, including Uttarakhand, Sikkim, and Arunachal Pradesh, to develop detailed Landslide Susceptibility Zonation (LSZ) models [23]. However, there is a need to assess the applicability of these techniques in the distinct geographical and climatic conditions of Spiti Valley.

This study aims to compare the Information Value (IV) and Frequency Ratio (FR) techniques in Spiti Valley using validation methods like Area Under the Curve (AUC) analysis and landslide density mapping. These validations will assess the accuracy of the LSZ models developed, providing insights into their effectiveness in predicting landslide susceptibility. The findings could inform mitigation strategies for government bodies, organizations, and future research efforts focused on enhancing landslide risk management in Spiti Valley.

## 2. Geological Landscape

Spiti, a high-altitude region in the Himalayas of northeastern Himachal Pradesh, India, is known as "The middle land" due to its location between Tibet and India. The study area encompasses the entire Spiti sub-division, including the upper Spiti Valley and extending to Sumdo [24]. The administrative centre is Kaza, situated at an elevation of 3,650 meters on the Spiti River's bank, while the district

headquarters is in Kyelang, Lahaul Valley [25]. Spiti and Lahaul are connected by NH-505 via Kunzum Pass at 4,590 meters, often closed by snow for 5-6 months annually [24]. The Spiti sub-division covers an area of 7,252,133,482 square meters and has a population of 12,445 according to the 2011 Census. Designated as a 'Tribal Area,' Spiti follows the Single-Line Administration system for direct communication between local and higher authorities.

Steep mountains, deep gorges, and a mix of braided and incised river channels characterise the valley's unique geography [25]. The Spiti River, originating from the base of the K-111 peak at 6,118 meters, flows through the valley, joined by major tributaries like the Pin and Lingti rivers [24]. The elevation in Spiti ranges from 2,325 meters to 6,558 meters, with its landscape transitioning from wide, braided river beds in the upper valley to deeply incised channels and gorges in the lower valley [24]. Spiti has a cold desert environment, marked by arid conditions due to its location in the rain shadow of the Himalayas. The region receives an average annual rainfall of about 50 mm, with snowfall typically less than 200 cm. Sporadically, there may be up to 15 mm of rainfall in a day, leading to erosion and landslides. The temperatures range from -25°C in winter to 15°C in summer. The region's aridity and extreme temperatures create a harsh environment with limited vegetation, primarily consisting of stunted willows and scattered shrubs in some villages.

Spiti Valley is situated in a seismically active zone, making it susceptible to earthquakes [12]. The area lies within the influence of the Main Central Thrust (MCT) and the Main Boundary Thrust (MBT), significant fault lines in the Himalayas [5,12]. These geological structures result in frequent seismic activity, contributing to the area's vulnerability to landslides. Historical records indicate that the region has experienced several significant earthquakes, with epicenters often located in the vicinity of the MCT and MBT fault zones. The seismic activity, combined with steep slopes and loose sedimentary deposits, exacerbates the landslide risk in Spiti.

Spiti's geology features visible sedimentary strata due to minimal vegetation, making it a prime location for geological studies [24]. Over millennia, the Spiti River and its tributaries, such as the Pin and Lingti rivers, have cut deep gorges into the uplifted sedimentary layers. The valley floor comprises ancient sedimentary deposits [26], with extensive scree slopes along the valley sides. The lower valley exhibits incised channels and gorges, indicative of neotectonic activity in recent geological history [27]. This complex geological framework contributes to the region's susceptibility to landslides and requires detailed landslide susceptibility zonation (LSZ) studies.

Despite its arid conditions, Spiti boasts more than 450 species of plants, including Seabuckthorn, Aconitum, and various herbs like Ephedra and Artemisia [28]. The high-altitude pastures support small bushes and grasses, providing habitats for wildlife such as the Siberian ibex, snow leopard, red fox, and Himalayan wolf. The avifauna includes species like the lammergeier, Himalayan griffon, golden eagle, and various rosefinches [29]. Spiti is home to the Pin Valley National Park and Kibber Wildlife Sanctuary, which protect the region's unique biodiversity [28]. The local Bhoti-speaking population of Spiti follows Tibetan Buddhism, with significant cultural and historical sites like the Tabo Monastery, built in 996 CE [30]. Traditional agriculture has shifted from subsistence to cash crops, and the region has become a popular destination for photography, homestay tourism, and various forms of adventure tourism, including winter sports. Major towns in the valley include Kaza, the largest settlement and administrative center, and Tabo, known for its ancient monastery [30]. Other notable villages are Dhankar, known for its monastery and fort, and Kibber, which is one of the highest inhabited villages in the world.

Spiti's remote and rugged terrain presents challenges for transportation and communication, but it also preserves the valley's unique cultural heritage and natural beauty. The distinct geographical and climatic conditions of Spiti Valley, characterized by its high-altitude desert environment and challenging terrain, underscore the importance of tailored LSZ modelling. This study area, with its unique landscape and minimal vegetation, presents a significant opportunity for detailed LSZ studies to effectively manage landslide risks and contribute to sustainable development in the region.

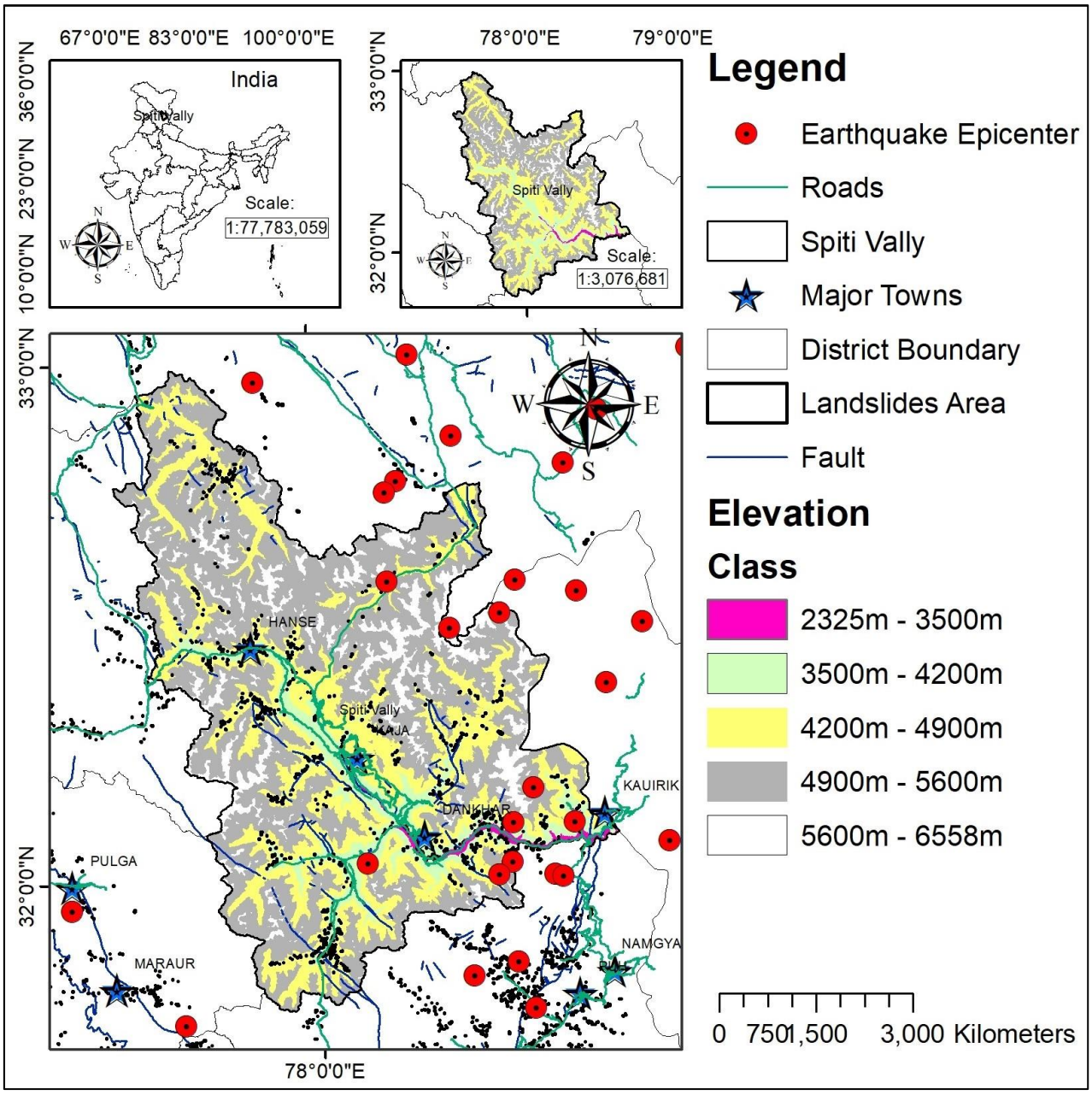


**Figure 2. Study Area Map.**

## 3. Material and Methods

The initial phase of this research project entails obtaining the necessary data, such as topographic, geological, soil, land use/land cover, climatic, hydrological, and seismic data, for the study area and creating a complete map database [31–33]. Data is compiled from a variety of sources: seismic data from the USGS, Digital Elevation Model (DEM) data from USGS, geological data and landslide inventory data from Bhuvan (further verified by Google Earth Pro imagery), due to the availability of accurate data on these different web portals. The DEM data provides important topographic parameters such as slope, aspect, curvature, elevation, stream density, Stream Power Index (SPI), and Topographic Wetness Index (TWI) for hydrological studies. Maps with a 30m-by-30m cell size are generated by converting DEM data to raster format, which are then used as inputs for landslip susceptibility study [34–37].

This analysis incorporates landslide conditioning factors (LCFs) such as slope, aspect, and curvature, employing the Information Value (IV) method [2–4,38] and Frequency Ratio (FR) methods [2,7,19–22] to compute landslide hazard zonation in the Spiti areas. Table 1 provides the lists of selected factors influencing landslide conditions, along with their respective data types and sources. These factors are instrumental in

landslide susceptibility analysis, offering valuable insights into terrain characteristics and anthropogenic influences within the study area.

A landslide susceptibility zonation (LSZ) map is a valuable tool for determining the risk of landslides in each location [15,32,39–41]. It entails compiling a complete dataset that includes geology, topography, satellite imaging, land use, rainfall, seismic, and historical landslip data. The data is then examined for Conditioning factors such as geological characteristics, slope, aspect, curvature, elevation, proximity to roads, rivers, faults, soil texture, Topographic Wetness Index (TWI), Topographic Roughness Index (TRI), road and stream density, land cover, rainfall intensity, proximity to water bodies, and seismic activity.

Using Geographic Information System (GIS) software like ArcGIS Pro 3.2.2, thematic maps for each causative factor are generated, creating a composite susceptibility map. Information value (IV) and Frequency ratio (FR) techniques are employed for data analysis, and separate models are prepared for each. The final LSZ map is validated using methods like AUC and Landslide Density [8]. Detailed steps of the methodology are shown in Figure 3 of the flowchart.

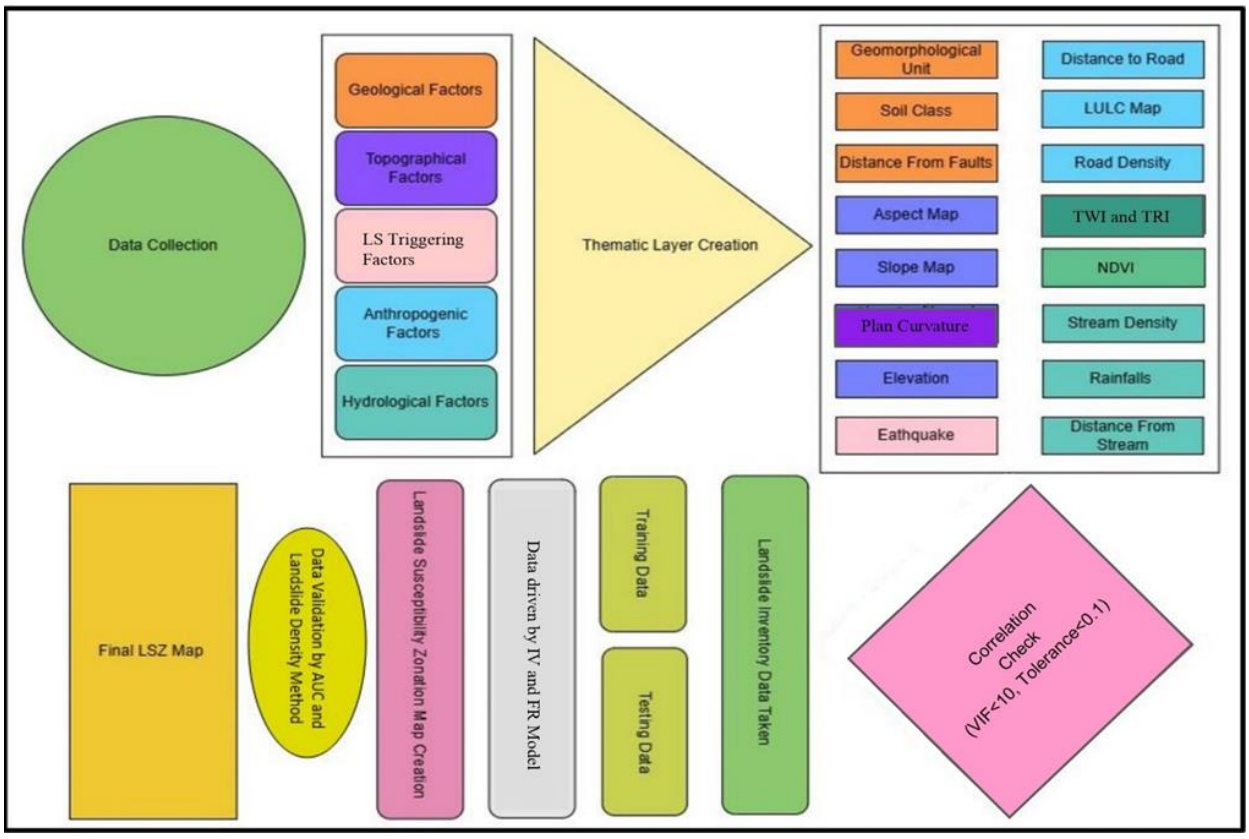


**Figure 3. Methodology Flow Chart.**

### 3.1. Landslide Inventory

A landslide inventory serves as a comprehensive record documenting past landslide occurrences within a specific area, encompassing details such as location, type, size, and triggering events [42,43]. It plays a crucial role in landslide susceptibility mapping, risk assessment, and land use planning by aiding stakeholders in identifying regions with high landslide activity frequencies and analyzing contributing factors [44–46]. This information facilitates informed decision-making to mitigate landslide hazards and minimize their impact on communities and infrastructure [47]. Additionally, a landslide inventory supports research and scientific studies on landslide processes, mechanisms, and impacts [48,49]. By continuously updating the inventory with new data, scholars and professionals can enhance their understanding of landslide mechanics and develop more effective landslide prevention and disaster management plans [50,51]. For the current study area, past landslide locations were gathered from various sources, including the Bhukosh-Geological Survey of India (GSI) website and Google Earth images [23,52,53]. These landslide events varied greatly, ranging from tens to thousands of square meters. However, for this study, the smallest landslide area identified measures 19.60 m², while the largest encompasses 76822.25 m², among a

total of 1314 landslide locations.

From all the identified landslides, approximately 93.37% (1226 landslides) are associated with rock movement, while the remaining 6.63% (87 landslides) are attributed to debris flow. Moreover, among all landslides, 98.09% (1288 landslides) occurred in barren land areas, 0.91% (12 landslides) in areas with sparse vegetation, 0.76% (10 landslides) in areas with thick vegetation, and 0.23% (3 landslides) in cultivated land areas. Subsequently, the training dataset was established, comprising 70% of the total landslide inventory. The remaining 30% was allocated for validation purposes, adhering to the widely adopted 70:30 ratio for the train-test split.[23]. This meticulous approach ensures robust model development and validation for effective landslide susceptibility assessment.

**Table 1. Lists spatial data sources used in this research and their collinearity statistics.**

| Factors | Data Type | Primary Data and its Source | Collinearity Statistics | |
|---|---|---|---|---|
| | | | Tolerance | VIF |
| SRTM DEM* | Continuous | USGS (30*30) | | |
| Road Networks** | Vector | Open Street map (vector) (https://www.openstreetmap.org/export | | |
| Faults Data*** | Vector | Fault shapefile downloaded from Bhukosh-GSI (1:50,000; vector) (https://bhukosh.gsi.gov.in/Bhukosh/Public) | | |
| Rainfall Data**** | Excel data | Climatic Research Unit (https://crudata.uea.ac.uk/cru/data/hrg) | | |
| Soil Data | Vector | FAO world soil map (1:5 M; vector) | | |
| Aspect | Continuous | Derived from DEM* | 0.860 | 1.163 |
| Plan Curvature | Continuous | Derived from DEM* | 0.881 | 1.135 |
| Slope | Continuous | Derived from DEM* | 0.793 | 1.261 |
| Elevation | Continuous | Derived from DEM* | 0.509 | 1.965 |
| TWI | Continuous | Derived from DEM* | 0.526 | 1.902 |
| Geomorphology Unit | Vector | Geomorphology map from Bhukosh-GSI (1:2 M; vector) | 0.590 | 1.694 |
| LULC | Discrete | Esri-landcover (10 m resolution; raster) | 0.477 | 2.098 |
| Rainfall | Continuous | Derived from Rainfall data**** | 0.625 | 1.600 |
| Earthquake | Continuous | USGS | 0.765 | 1.316 |
| DFF | Continuous | Derived from faults data*** | 0.565 | 2.150 |
| DFS | Continuous | Stream network map derived using DEM* | 0.886 | 1.929 |
| DFR | Continuous | Derived from Road Networks** | 0.763 | 2.315 |
| Road Density | Classified | Derived from DEM* | 0.850 | 1.305 |
| Stream Density | Classified | Stream network map derived using DEM* | 0.241 | 4.548 |
| Soil Texture | Discrete | Soil Data | 0.915 | 1.292 |
| NDVI | Discrete | NASA Earth Data Portal | 0.760 | 1.415 |
| TRI | Continuous | SRTM DEM* | 0.748 | 1.839 |

### 3.2. Conditioning factors

Numerous factors, including human activity levels, occurrences of natural disasters like earthquakes, and prevailing geoenvironmental conditions, often influence the frequency of landslides in any given area. Landslide Susceptibility Studies (LSS) have no set rules for determining influencing factors [3,6,15,22,54–56]. Instead, these factors are selected based on regional characteristics and data availability. As supported by existing literature and research findings, topography, geology, hydrology, vegetation, climate, and human activities all play significant roles. These elements collectively shape the physical and environmental characteristics of a location. Thus, this study divides causative elements into five categories: geological, topographical, triggering, anthropogenic, and hydrological factors. The rationale for selecting specific factors in the Frequency Ratio (FR) and Information Value (IV) models is based on their demonstrated relevance and statistical significance in past studies. Factors such as slope angle, rainfall intensity, and land cover type were specifically chosen due to their well-documented impact on landslide occurrences. Slope angle is a critical factor as steeper slopes are more prone to failure. Rainfall intensity influences the saturation of soil and slope stability, making it a key triggering factor. Land cover type affects soil cohesion and runoff patterns, thereby impacting susceptibility.

#### 3.2.1. Landslide-trigging Factors

Landslide-triggering factors in the Spiti Valley

encompass earthquake events and rainfall intensity [57–61], both of which are crucial in assessing landslide susceptibility. Earthquakes, classified into five magnitude classes (0-2, 2-3, 3-4, 4-5, and 5-6) based on the Richter scale of earthquake intensity, are sourced from the United States Geological Survey (USGS). These seismic events contribute significantly to slope instability by inducing ground shaking and potentially destabilizing already vulnerable terrain.

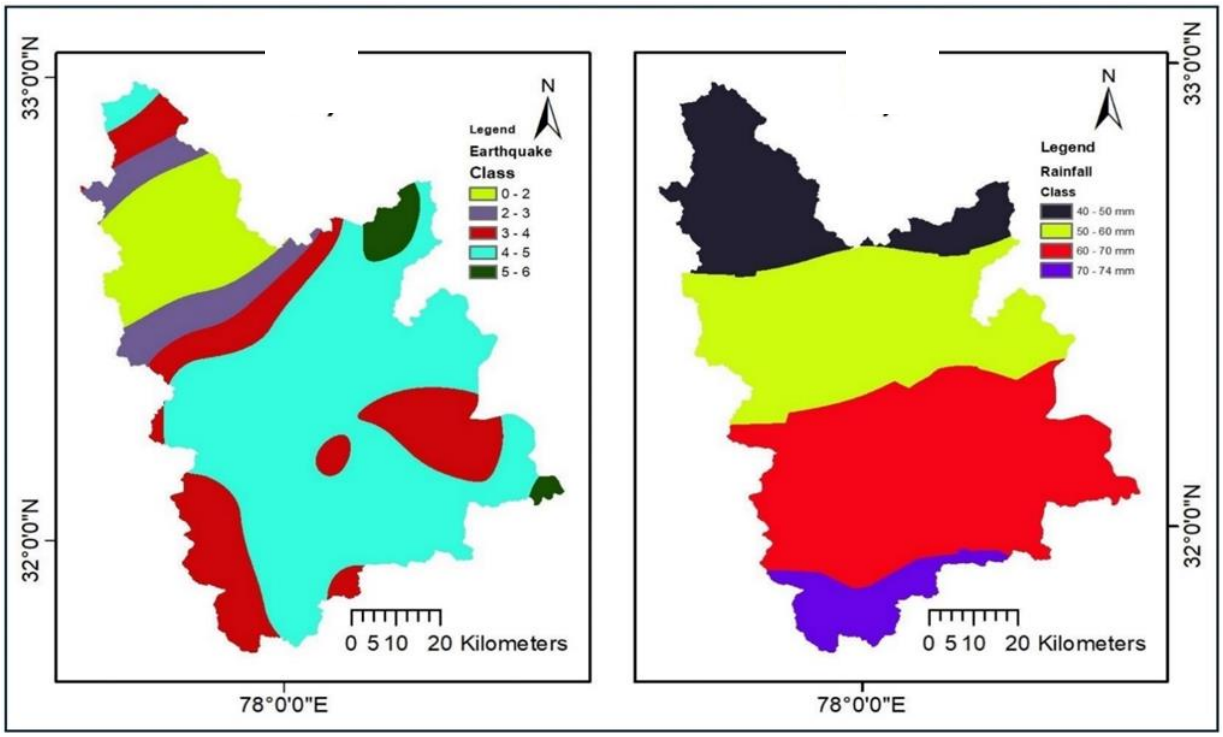


**Figure 4. Landslide Triggering Factors Thematic Layer a) Earthquake, b) Rainfalls**.

Rainfall intensity, classified into five categories ranging from 40-50mm to 70-74mm, plays a pivotal role in triggering landslides. Higher-intensity rainfall events can saturate soils, increase pore water pressure, and initiate mass movements on steep slopes [37,62]. The data for rainfall events spanning from 1990 to 2023 was obtained from the Climatic Research Unit (CRU) at the University of East Anglia (UEA). Understanding these triggering factors is essential for accurately predicting landslide susceptibility in the Spiti Valley, enabling effective disaster risk management strategies and land use planning to mitigate potential hazards.

### 3.2.2. Geological Factors

Geological factors play a pivotal role in assessing landslide susceptibility in the study area, encompassing geomorphological units (GU), soil texture (ST), and distance from faults (DFF) [21,63–65]. The geomorphological units provide crucial insights into the landscape's stability [66], delineating areas such as DenOri - Piedmont Slope and GlaOri - Glacial Terrain, each characterized by distinct physical and chemical properties influenced by past geological processes [24]. Soil texture variations, predominantly loam and UWB, further influence slope stability due to their permeability and shear strength characteristics, affecting how water and stresses interact within the terrain. Moreover, the proximity to faults, categorized into zones ranging from <500m to >2500m using Euclidean distance analysis, highlights areas vulnerable to seismic activity and potential landslide initiation points. Together, these geological factors offer a comprehensive framework for understanding the spatial distribution of landslide susceptibility, essential for effective hazard assessment and mitigation strategies in the region.

Integrating data from the FAO platform for soil texture mapping and utilizing spatial analytical tools for fault distance categorization have enhanced the accuracy of landslide susceptibility assessments [14]. Combining these geological factors such as GU, ST, and DFF are essential for predicting LSZ in the Spiti Valley. The detailed characterization of GU, including DenOri - Piedmont Slope and GlaOri - Glacial Terrain, alongside soil textures like loam and UWB,

provides critical insights into slope stability dynamics. Understanding the proximity to faults, categorized into zones from <500m to >2500m, using spatial analytical tools further enhances the assessment of landslide risks. This comprehensive analysis informs the development of LSZ maps, crucial for sustainable land use planning and disaster risk management in the region. By integrating these geological factors, this study aims to predict and map LSZ effectively, supporting targeted interventions to mitigate landslide hazards and enhance resilience in the Spiti Valley.

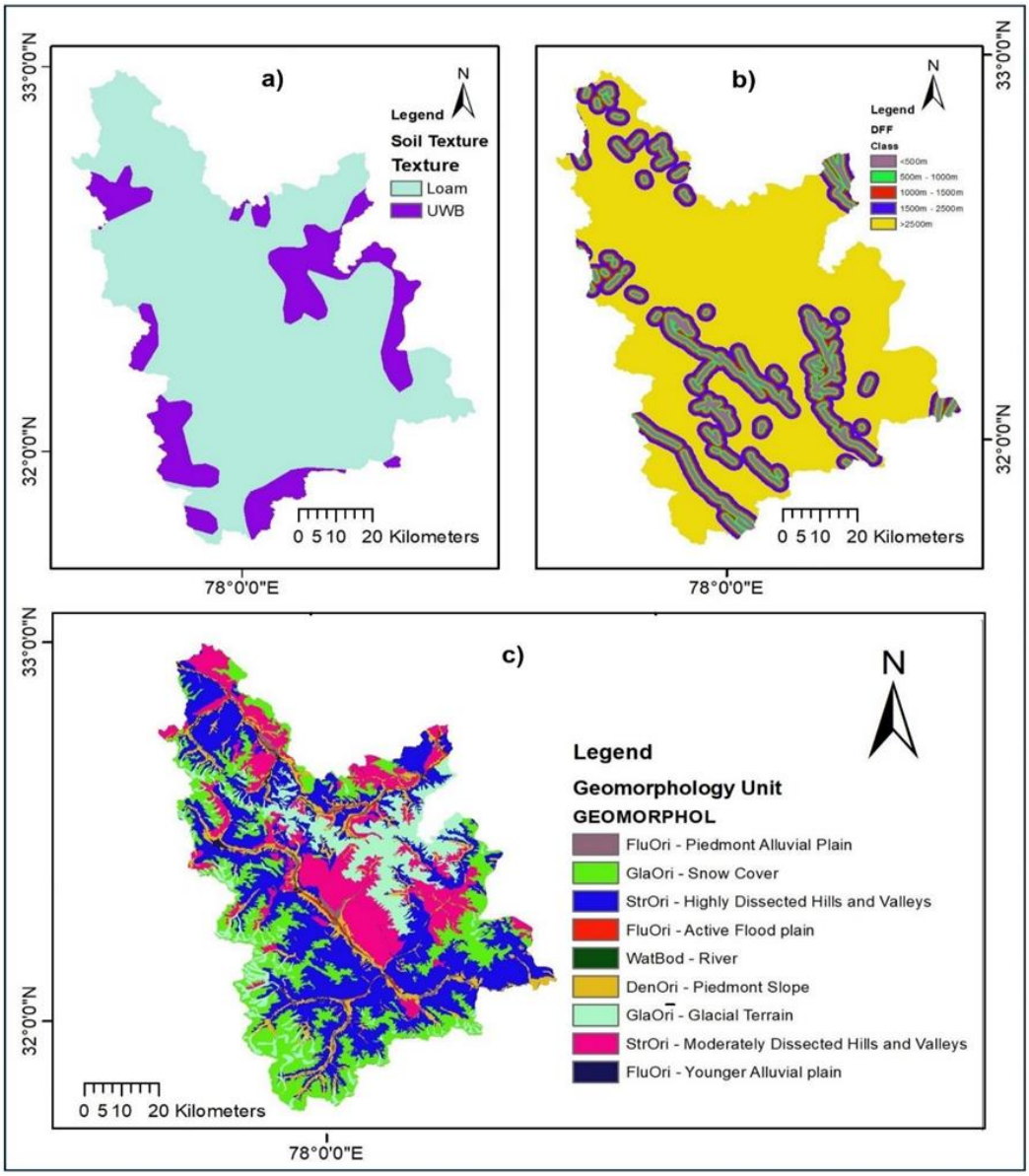


**Figure 5. Geological Conditioning factors Thematic Layers. a) Distance from Fault, b) Soil Texture, c) Geomorphological Unit.**

### 3.2.3. Anthropogenic Factors

The Normalized Difference Vegetation Index (NDVI) signifies vegetation cover and health [67–69]. It is calculated using high-resolution Sentinel-2 multispectral imagery with the formula:

$$NDVI = (NIR - R)/(NIR + R),$$

where NIR and R represent the near-infrared and red bands, respectively [23,70].

The NDVI values are reclassified into five categories: <0, 0-0.2, 0.2-0.4, 0.4-0.6, and 0.6-1. Dense vegetation can stabilize slopes by reinforcing soil with roots and reducing surface runoff, while sparse vegetation can increase landslide susceptibility. Land Use Land Cover (LULC) is another crucial factor in landslide susceptibility studies [23,40,71,72]. The LULC map for the study area categorizes the land into various classes: water (1), tree (2), flooded vegetation (3), crop (4), built area (5), bare ground

(6), snow/ice (7), and rangeland (8). Each class has different implications for slope stability. For example, built areas and bare ground are more prone to landslides due to reduced natural vegetation, while tree and rangeland areas may offer more stability due to better root structure and soil reinforcement.

The distance from roads (DFR) is another key factor affecting landslide susceptibility. Roads can alter natural drainage patterns and slope stability, making areas near roads more susceptible to landslides [73–75]. This study classified the distance from roads into five zones: <100m, 100-500m, 500-1000m, 1000-1500m, and >1500m. Understanding the impact of proximity to roads on slope stability is essential for infrastructure planning and landslide risk management in the region [76]. Road density (RD) is another critical factor, indicating the intensity of road networks in an area [75,77–79]. High road density can exacerbate landslide risks due to increased human activity and alterations in natural drainage [80]. The road density for the study area is calculated using the kernel density tool and classified into five classes: 0-0.16, 0.16-0.35, 0.35-0.50, 0.50-0.64, and 0.64-0.83. This classification helps in identifying areas with varying degrees of risk related to road density, further contributing to comprehensive landslide susceptibility mapping.

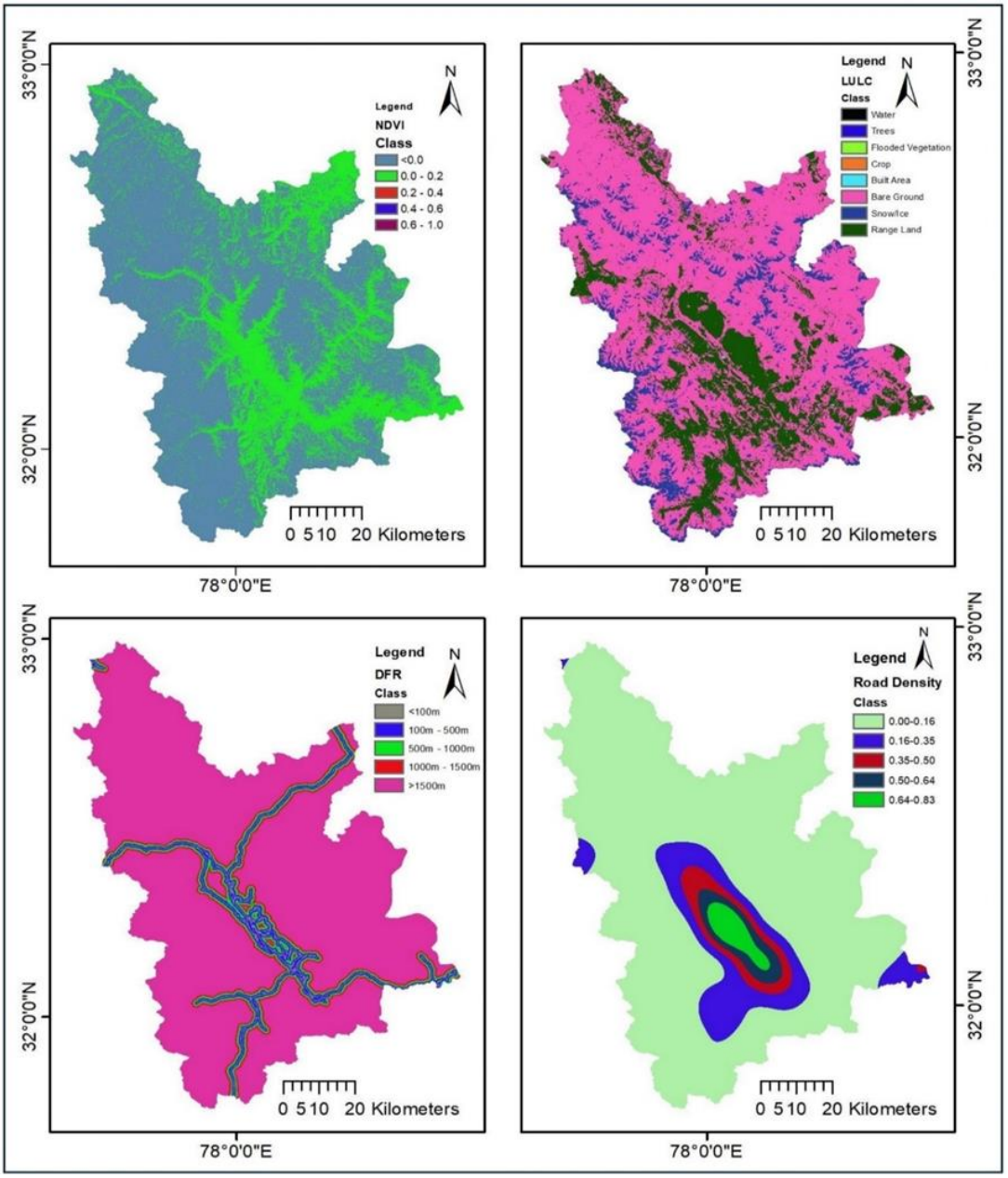


**Figure 6. Anthropogenic Conditioning factors Thematic Layers a) NDVI, b) Land Use Land Cover (LULC), c) Distance from Roads (DFR) d) Road Density.**

### 3.2.4. Topographic Factors

Topographical factors significantly influence slope stability and are crucial for assessing landslide susceptibility [9,81,82]. Key topographical factors include slope, aspect, plan curvature, profile curvature, and elevation [83–86]. The geospatial database of these topographical factors with 30 m spatial resolution, is prepared using GIS with UTM Zone 43S projected coordinate system and WGS 1984 datum. Elevation, plan curvature, slope angle, and aspect are extracted using the digital elevation model (DEM) taken from the USGS database with less than 10% cloud coverage.

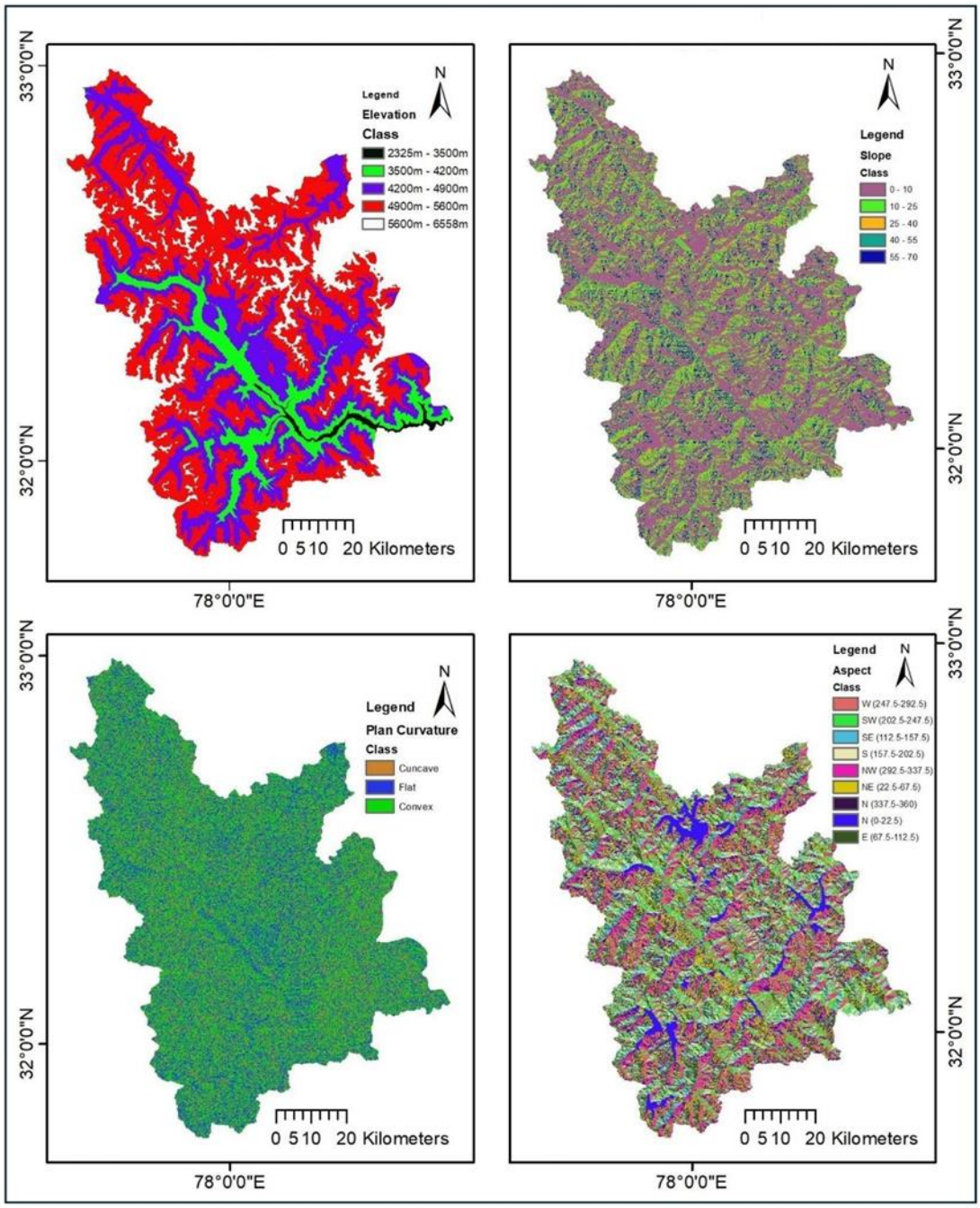


**Figure 7. Topographical Conditioning factors Thematic Layers a) Elevation b) Slope, c) Plan Curvature d) Aspect.**

Elevation is classified into five categories: 2325-3500 m, 3500-4200 m, 4200-4900 m, 4900-5600 m, and 5600-6558 m. Higher elevations typically experience more severe weather conditions, including higher precipitation and stronger winds, which contribute to erosion and slope instability [87–89]. Additionally, higher areas might have different soil types and vegetation

cover compared to lower elevations, influencing their susceptibility to landslides [90–92]. Slopes are also classified into five categories with ranges of 0-10 degrees, 10-25 degrees, 25-40 degrees, 40-55 degrees, and 55-70 degrees. Steeper slopes are more prone to landslides due to the increased gravitational force acting on the slope material, making them less stable compared to gentler slopes.

Plan curvature is classified into three categories: concave, flat, and convex. Concave slopes tend to accumulate water, increasing the risk of landslides [7,61], while convex slopes may shed water more effectively [75]. Aspect, indicating the direction the slope faces, is classified into nine categories: West (247.5-292.5 degrees), Southwest (202.5-247.5 degrees), Southeast (112.5-157.5 degrees), South (157.5-202.5 degrees), Northwest (292.5-337.5 degrees), Northeast (22.5-67.5 degrees), North (337.5-360 degrees), North (0-22.5 degrees), and East (67.5-112.5 degrees). Aspect affects the amount of sunlight and moisture the slope receives, influencing soil moisture content and vegetation growth, both of which impact slope stability [64,93,94]. For instance, slopes facing the sun might dry out faster, reducing soil cohesion, while shaded slopes might retain moisture, increasing the risk of saturation and instability [32,69,73].

These topographical factors are integral to landslide susceptibility zoning (LSZ) as they provide a detailed understanding of the terrain's physical characteristics [61,89]. By analyzing these factors, we can identify areas at higher risk of landslides, enabling more effective land use planning and disaster risk management strategies.

### 3.2.5. Hydrological Factors

Hydrological factors derived from the Digital Elevation Model (DEM) play a significant role in assessing landslide susceptibility in the study area [5,89]. The Topographic Wetness Index (TWI) is calculated using the formula $TWI = \ln (AS/\tan \beta)$, where AS is the specific contributing area and β is the slope angle [3,23,47,66]. TWI values, indicating the potential for water accumulation, are classified into five categories: 4-6, 6-12, 12-18, 18-25, and 25-32. Higher TWI values suggest areas prone to water saturation and increased landslide risk due to enhanced moisture content [78,86,93].

The Topographic Roughness Index (TRI) assesses terrain ruggedness based on the variation in elevation [95,96]. It is calculated as (DEMmean - DEMmin) / (DEMmax - DEMmin), where DEMmean, DEMmin, and DEMmax are the mean, minimum, and maximum elevations, respectively [36,79,97,98]. TRI values ranging from 0 to 1, are reclassified into five categories: 0-0.2, 0.2-0.4, 0.4-0.6, 0.6-0.8, and 0.8-1.0. Higher TRI values indicate more rugged terrain, influencing water flow patterns and contributing to localized areas of water accumulation and potential instability. Distance from Stream (DFS) categorizes proximity to streams, critical for understanding moisture availability and erosion potential [46]. DFS is classified into five zones: <300m, 300-500m, 500-1000m, 1000-1500m, and >1500m. Areas closer to streams are more susceptible to increased moisture levels and erosion, impacting slope stability during intense rainfall events.

Stream Density (SD) measures the total length of streams per unit area and reflects drainage network complexity [62]. SD values, ranging from 0.00 to 1.20, are categorized into five classes: 0.00-0.25, 0.25-0.50, 0.50-0.75, 0.75-0.95, and 0.95-1.20. Higher SD values indicate a denser drainage network, influencing water flow dynamics and sediment transport, which are critical factors in landslide initiation and propagation [41,47,66]. Integrating these hydrological factors with geological and topographical data provides a comprehensive approach to landslide susceptibility mapping (LSZ), facilitating effective land use planning and disaster risk management strategies in the study area.

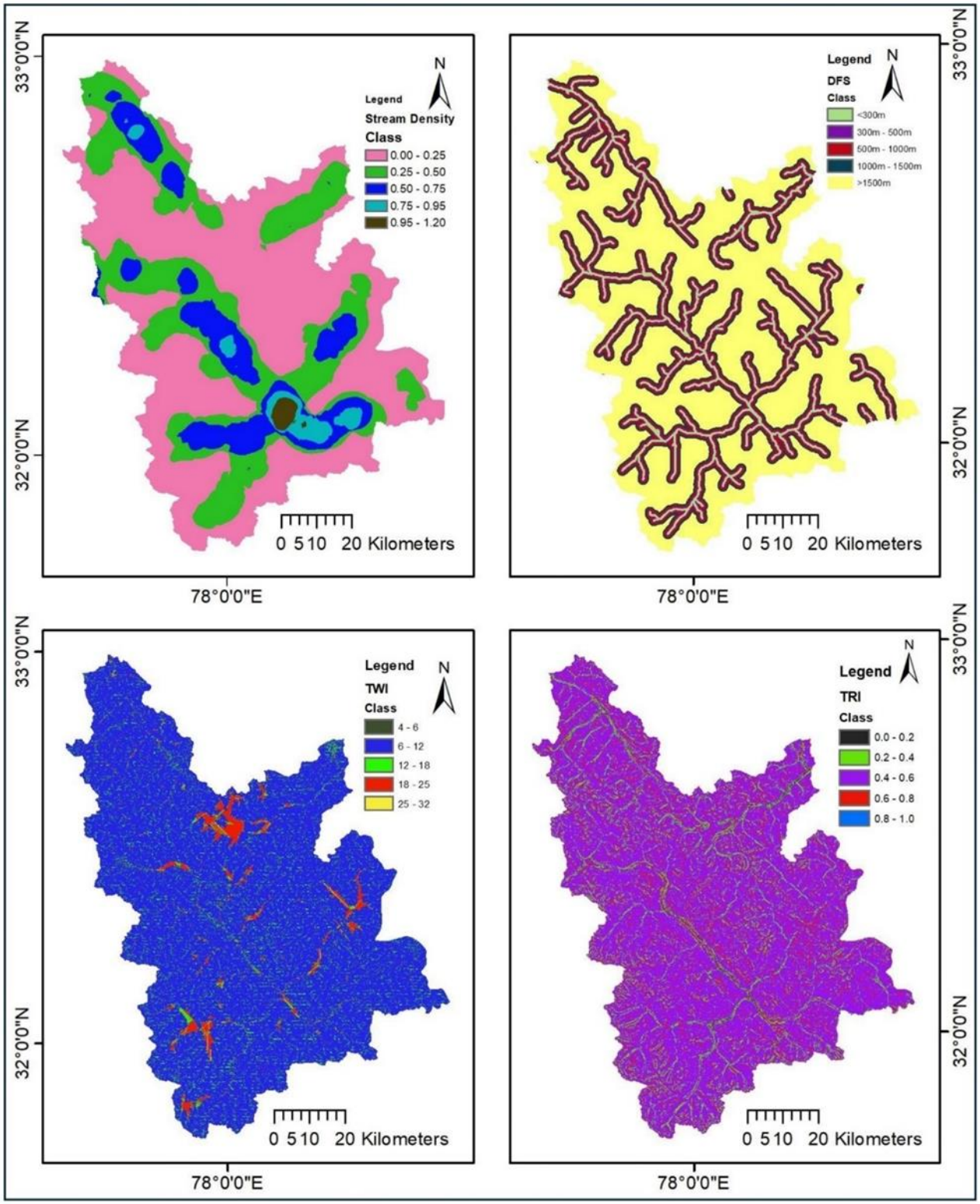


**Figure 8. Hydrological Conditioning factors Thematic Layers a) Stream Density, b) Distance from Stream, c) Topographic Wetness Index (TWI), d) Topographic Roughness Index (TRI).**

### 3.3. Multicollinearity analysis of Conditioning factors

After preparing all the thematic layer of conditioning factors, it was analysed for collinearity. To analyze the theses, 200 spatially balance points were created with the tool in ArcGIS Pro 3.2. Then all the thematic layers (conditioning factors data were extracted to this point with the help of extract multi values to point tools. Then it is exported on csv file. Then its Collinearity Statistics were checked by BIM SPSS

Software. VIF and These conditioning factors were analyzed using Collinearity Statistics, such as Variance Inflation Factor (VIF) and tolerance (T). A VIF value greater than 10 and tolerance less than 0.1 indicates the problem of multicollinearity between landslide conditioning factors (LCFs). Therefore, only factors with a VIF value less than 10 and tolerance greater than 0.1 were chosen for this study. By incorporating these factors, we ensure a comprehensive assessment of landslide susceptibility that reflects both regional characteristics and established scientific findings. This selection enhances the robustness of the FR and IV models, providing a more accurate prediction of landslide-prone areas.

## 4. Result and discussion

### 4.1. Frequency Ratio (FR)

The Frequency Ratio (FR) method is a bivariate statistical approach used to evaluate landslide susceptibility by analyzing the relationship between the spatial distribution of landslides and various contributing factors [84,99]. This method calculates the ratio of the probability of landslide occurrence to the probability of non-occurrence for different factor classes. The formula for the FR method is:

$$FR = (Si/Ni)/(S/N)$$

Where: Si is the number of landslide pixels in a given factor class,

Ni is the total number of pixels in that factor class,

S is the total number of landslide pixels in the entire study area and

N is the total number of pixels in the study area.

A FR value greater than 1 indicates a higher likelihood of landslide occurrence in that particular factor class, while a FR value less than 1 suggests a lower likelihood [7,20–22]. In the study area, the FR method was applied to various geomorphological, topographical, and hydrological factors. For instance, highly dissected hills and valleys showed an FR of 1.5711, indicating a high susceptibility, while glacial terrain had an FR of 0.0000, indicating low susceptibility. Similarly, land use types like bare ground and aspect classes such as southeast-facing slopes had higher FR values of 1.1421 and 1.5668, respectively. Other factors such as soil type, rainfall, stream density, road density, slope, terrain ruggedness index (TRI), plan curvature, topographic wetness index (TWI), earthquake intensity, normalized difference vegetation index (NDVI), elevation, distance from roads, faults, and streams were also analyzed, and their FR values were calculated (see Table 2).

These FR values were then used to interpret the thematic layers with a lookup tool. By combining these data in ArcGIS Pro 3.3 with the help of raster calculation, an FR-based landslide susceptibility zoning (LSZ) model was prepared. This model categorizes the landscape into five susceptibility classes: Low, Moderate, High, Very High, and Extremely High. This classification provides a detailed and concise representation of landslide susceptibility, aiding in effective land-use planning and disaster management.

### 4.2. Information Value (IV)

IV method is also a spatial bivariate statistical approach for predicting landslide events by analyzing the relationship between landslide occurrences and various Conditioning factors [2,3,16]. This method calculates the information value for each factor class based on the presence of landslides. The IV for a given factor class is computed using the formula:

$$IV = \log((Si/Ni)/(S/N)),$$

Where, Si is the number of landslide pixels in the factor class,

Ni is the area of the factor class,

S is the total number of landslide pixels in the entire study area and

N is the total number of pixels in the entire study area.

An IV greater than 0 indicates a positive correlation with landslide occurrence, while an IV less than 0 indicates a negative correlation [3,4]. In this study, the IV method was applied to various geomorphological, topographical, and hydrological factors. For example, highly dissected hills and valleys had an IV of 0.4518, indicating a strong correlation with landslide occurrence, while glacial terrain had an IV of 0, showing no correlation. Other factors like land use, soil type, rainfall, stream density, road density, slope, TRI, plan curvature, TWI, earthquake intensity, NDVI, elevation, and distances from roads, faults, and streams were also analyzed (see Table 2). The IV values helped determine the intensity of each factor's contribution to landslide susceptibility.

These IV values were then used to interpret the thematic layers using a lookup tool. By combining these data in ArcGIS Pro 3.3 with the help of raster calculation, an IV-based landslide susceptibility zoning (LSZ) model was prepared. This model

categorized the study area into five susceptibility classes: Low, Moderate, High, Very High, and Extremely High. This classification aids in understanding the spatial distribution of landslide risk, thus facilitating effective land-use planning and disaster management in the study area.

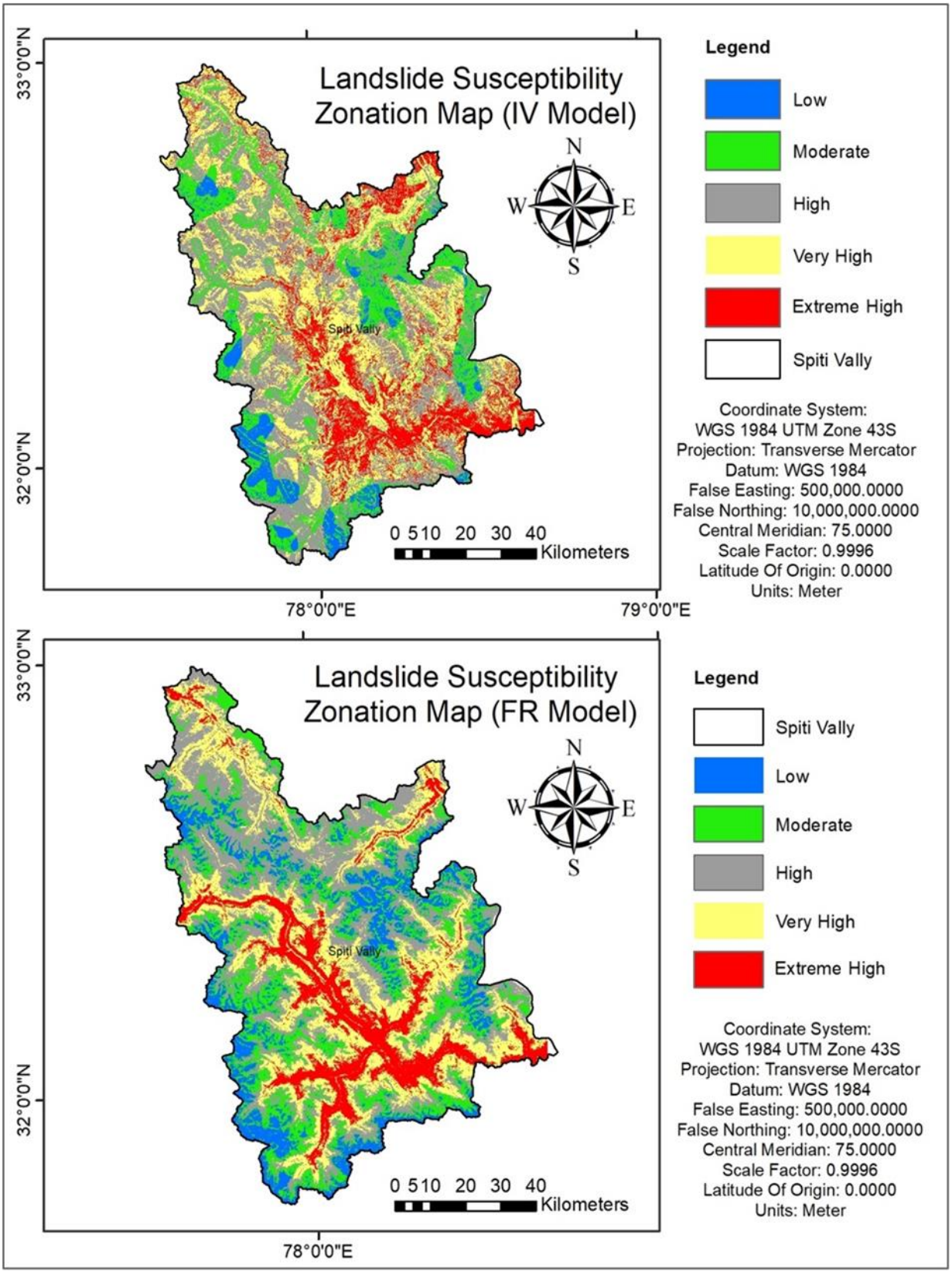


**Figure 10. LSZ of IV and FR models.**

**Table 2. LS factors and its FR and IV value**

| ID | LS Factors | Class | Ni | Ni% | Si | Si% | FR | IV |
|---|---|---|---|---|---|---|---|---|
| 1 | GU | FluOri - Piedmont Alluvial Plain | 82749 | 1.03% | 28 | 1.00% | 0.9673 | -0.0333 |
| | | GlaOri - Snow Cover | 1732879 | 21.60% | 4 | 0.14% | 0.0066 | -5.0209 |
| | | StrOri - Highly Dissected Hills and Valleys | 2956700 | 36.86% | 1625 | 57.91% | 1.5711 | 0.4518 |
| | | FluOri - Active Flood plain | 53993 | 0.67% | 2 | 0.07% | 0.1059 | -2.2454 |
| | | WatBod - River | 85278 | 1.06% | 24 | 0.86% | 0.8045 | -0.2175 |
| | | DenOri - Piedmont Slope | 643974 | 8.03% | 529 | 18.85% | 2.3483 | 0.8537 |
| | | GlaOri - Glacial Terrain | 1069665 | 13.34% | 0 | 0.00% | 0.0000 | 0.0000 |
| | | StrOri - Moderately Dissected Hills and Valleys | 1375161 | 17.14% | 590 | 21.03% | 1.2265 | 0.2041 |
| | | FluOri - Younger Alluvial plain | 20981 | 0.26% | 4 | 0.14% | 0.5450 | -0.6070 |
| | | **N = 8021380** | | **S = 2806** | | | | |
| 2 | LULC | Water 4058 | | 0.05% | 1 | 0.04% | 0.7044 | -0.3503 |
| | | Trees | 3 | 0.00% | 0 | 0.00% | 0.0000 | 0.0000 |
| | | Flooded Vegetation | 303 | 0.00% | 0 | 0.00% | 0.0000 | 0.0000 |
| | | Crop | 60 | 0.00% | 0 | 0.00% | 0.0000 | 0.0000 |
| | | Built Area | 1980 | 0.02% | 0 | 0.00% | 0.0000 | 0.0000 |
| | | Bare Ground | 5494088 | 68.49% | 2195 | 78.23% | 1.1421 | 0.1329 |
| | | Snow/Ice | 738423 | 9.21% | 0 | 0.00% | 0.0000 | 0.0000 |
| | | Range Land | 1782465 | 22.22% | 610 | 21.74% | 0.9783 | -0.0219 |
| 3 | Aspect | North (0-22.5) | 771956 | 9.62% | 325 | 11.58% | 1.2035 | 0.1852 |
| | | NorthEast (22.5-67.5) | 1088866 | 13.57% | 308 | 10.98% | 0.8086 | -0.2124 |
| | | East (67.5-112.5) | 1152517 | 14.37% | 424 | 15.11% | 1.0517 | 0.0504 |
| | | SouthEast (112.5-157.5) | 863008 | 10.76% | 473 | 16.86% | 1.5668 | 0.4490 |
| | | South (157.5-202.5) | 832469 | 10.38% | 349 | 12.44% | 1.1984 | 0.1810 |
| | | SouthWest (202.5-247.5) | 1009328 | 12.58% | 440 | 15.68% | 1.2462 | 0.2201 |
| | | West (247.5-292.5) | 1048447 | 13.07% | 274 | 9.76% | 0.7471 | -0.2916 |
| | | NorthWest (292.5-337.5) | 835413 | 10.41% | 141 | 5.02% | 0.4825 | -0.7288 |
| | | North (337.5-360) | 419376 | 5.23% | 72 | 2.57% | 0.4908 | -0.7118 |
| 4 | Soil Type | Loam | 6540023 | 81.53% | 2691 | 95.90% | 1.1762 | 0.1623 |
| | | UWB | 1481357 | 18.47% | 115 | 4.10% | 0.2219 | -1.5054 |
| 5 | Rainfalls | 40 - 50 mm | 1487060 | 18.54% | 431 | 15.36% | 0.8285 | -0.1881 |
| | | 50 - 60 mm | 2581797 | 32.19% | 706 | 25.16% | 0.7817 | -0.2463 |
| | | 60 - 70 mm | 3414948 | 42.57% | 1568 | 55.88% | 1.3126 | 0.2720 |
| | | 70 - 74 mm | 537575 | 6.70% | 101 | 3.60% | 0.5371 | -0.6216 |
| 6 | Stream Density | 0.00 - 0.25 | 4582242 | 57.13% | 623 | 22.20% | 0.3887 | -0.9450 |
| | | 0.25 - 0.50 | 2225370 | 27.74% | 1029 | 36.67% | 1.3218 | 0.2790 |
| | | 0.50 - 0.75 | 972672 | 12.13% | 776 | 27.66% | 2.2806 | 0.8245 |
| | | 0.75 - 0.95 | 184239 | 2.30% | 335 | 11.94% | 5.1979 | 1.6482 |
| | | 0.95 - 1.20 | 56857 | 0.71% | 43 | 1.53% | 2.1620 | 0.7710 |
| 7 | Road Density | 0.00-0.16 | 6592199 | 82.18% | 2050 | 73.06% | 0.8890 | -0.1177 |
| | | 0.16-0.35 | 843897 | 10.52% | 518 | 18.46% | 1.7547 | 0.5623 |
| | | 0.35-0.50 | 257922 | 3.22% | 151 | 5.38% | 1.6736 | 0.5150 |
| | | 0.50-0.64 | 178003 | 2.22% | 42 | 1.50% | 0.6745 | -0.3938 |
| | | 0.64-0.83 | 149359 | 1.86% | 45 | 1.60% | 0.8613 | -0.1493 |
| 8 | Slope | 0 - 10 | 3996096 | 49.82% | 1867 | 66.54% | 1.3356 | 0.2894 |
| | | 10 - 20 | 1308725 | 16.32% | 284 | 10.12% | 0.6203 | -0.4775 |
| | | 25 - 40 | 1198875 | 14.95% | 268 | 9.55% | 0.6390 | -0.4478 |
| | | 40 - 55 | 851741 | 10.62% | 187 | 6.66% | 0.6276 | -0.4658 |
| | | 55 - 70 | 665943 | 8.30% | 200 | 7.13% | 0.8585 | -0.1525 |
| 9 | TRI | 0.0 - 0.2 | 19610 | 0.24% | 0 | 0.00% | 0.0000 | 0.0000 |
| | | 0.2 - 0.4 | 1015901 | 12.66% | 261 | 9.30% | 0.7344 | -0.3087 |
| | | 0.4 - 0.6 | 6324654 | 78.85% | 2334 | 83.18% | 1.0549 | 0.0535 |
| | | 0.6 - 0.8 | 659898 | 8.23% | 211 | 7.52% | 0.9140 | -0.0899 |
| | | 0.8 - 1.0 | 1317 | 0.02% | 0 | 0.00% | 0.0000 | 0.0000 |
| 10 | Pln_C | Cuncave | 1194233 | 14.89% | 542 | 19.32% | 1.2974 | 0.2604 |
| | | Flat | 3360253 | 41.89% | 890 | 31.72% | 0.7571 | -0.2782 |
| | | Convex | 3466894 | 43.22% | 1374 | 48.97% | 1.1329 | 0.1248 |

**Continues of Table 2. LS factors and its FR and IV value**

| ID | LS Factors | Class | Ni | Ni% | Si | Si% | FR | IV |
|---|---|---|---|---|---|---|---|---|
| 11 | TWI | 4 - 6 | 462 | 0.01% | 0 | 0.00% | 0.0000 | 0.0000 |
| | | 6 - 12 | 7028860 | 87.63% | 2401 | 85.57% | 0.9765 | -0.0238 |
| | | 12 - 18 | 719205 | 8.97% | 207 | 7.38% | 0.8228 | -0.1951 |
| | | 18 - 25 | 260136 | 3.24% | 190 | 6.77% | 2.0879 | 0.7362 |
| | | 25 - 32 | 12717 | 0.16% | 8 | 0.29% | 1.7983 | 0.5869 |
| 12 | EQ | 0 - 2 | 1030619 | 12.85% | 216 | 7.70% | 0.5991 | -0.5123 |
| | | 2 - 3 | 583458 | 7.27% | 150 | 5.35% | 0.7349 | -0.3080 |
| | | 3 - 4 | 1737986 | 21.67% | 366 | 13.04% | 0.6020 | -0.5075 |
| | | 4 - 5 | 4468189 | 55.70% | 1914 | 68.21% | 1.2245 | 0.2026 |
| | | 5 - 6 | 201128 | 2.51% | 160 | 5.70% | 2.2741 | 0.8216 |
| 13 | NDVI | <0.0 | 5566623 | 69.40% | 890 | 31.72% | 0.4570 | -0.7830 |
| | | 0.0 - 0.2 | 2453650 | 30.59% | 1916 | 68.28% | 2.2323 | 0.8030 |
| | | 0.2 - 0.4 | 1057 | 0.01% | 0 | 0.00% | 0.0000 | 0.0000 |
| | | 0.4 - 0.6 | 35 | 0.00% | 0 | 0.00% | 0.0000 | 0.0000 |
| | | 0.6 - 1.0 | 15 | 0.00% | 0 | 0.00% | 0.0000 | 0.0000 |
| 14 | Elevation | 2325m - 3500m | 85847 | 1.07% | 117 | 4.17% | 3.8960 | 1.3600 |
| | | 3500m - 4200m | 755049 | 9.41% | 985 | 35.10% | 3.7293 | 1.3162 |
| | | 4200m - 4900m | 2439116 | 30.41% | 1274 | 45.40% | 1.4931 | 0.4009 |
| | | 4900m - 5600m | 3957721 | 49.34% | 429 | 15.29% | 0.3099 | -1.1716 |
| | | 5600m - 6558m | 783647 | 9.77% | 1 | 0.04% | 0.0036 | -5.6136 |
| 15 | Distance from Road | <100m | 127351 | 1.59% | 43 | 1.53% | 0.9652 | -0.0354 |
| | | 100m - 500m | 344923 | 4.30% | 276 | 9.84% | 2.2874 | 0.8274 |
| | | 500m - 1000m | 337309 | 4.21% | 300 | 10.69% | 2.5425 | 0.9331 |
| | | 1000m - 1500m | 295424 | 3.68% | 391 | 13.93% | 3.7835 | 1.3306 |
| | | >1500m | 6916373 | 86.22% | 1796 | 64.01% | 0.7423 | -0.2980 |
| 16 | Distance from Faults | <500m | 475492 | 5.93% | 209 | 7.45% | 1.2565 | 0.2283 |
| | | 500m - 1000m | 504357 | 6.29% | 256 | 9.12% | 1.4510 | 0.3722 |
| | | 1000m - 1500m | 490937 | 6.12% | 118 | 4.21% | 0.6871 | -0.3753 |
| | | 1500m - 2500m | 946937 | 11.81% | 363 | 12.94% | 1.0958 | 0.0915 |
| | | >2500m | 5603657 | 69.86% | 1860 | 66.29% | 0.9489 | -0.0525 |
| 17 | Distance from Stream | <300m | 673312 | 8.39% | 863 | 30.76% | 3.6640 | 1.2986 |
| | | 300m - 500m | 404235 | 5.04% | 331 | 11.80% | 2.3408 | 0.8505 |
| | | 500m - 1000m | 1004906 | 12.53% | 636 | 22.67% | 1.8092 | 0.5929 |
| | | 1000m - 1500m | 951172 | 11.86% | 400 | 14.26% | 1.2022 | 0.1841 |
| | | >1500m | 4987755 | 62.18% | 576 | 20.53% | 0.3301 | -1.1083 |

### 4.3. Validation

The validation of the landslide susceptibility models was conducted using two primary methods: Receiver Operating Characteristic (ROC) curves/Area Under the Curve (AUC) values and the Landslide Density Index (LDI) method. These approaches ensured a comprehensive assessment of the model's predictive accuracy and reliability. Among the 1,313 landslide locations, there were 4,007 pixels (30x30). There was no strict rule for the training and testing ratio in this study; 70% of training data (2,806 pixels) was taken for model prediction, and 30% of testing data (1,199 pixels) was taken for validation. Both the Frequency Ratio (FR) and Information Value (IV) models were evaluated using these methods, yielding high AUC values that demonstrated their strong predictive performance. The AUC values obtained were 84.1 for the FR model and 83.9 for the IV model, indicating strong predictive performance for both models. The Landslide Density Index (LDI) method provided additional validation by examining the spatial distribution of landslides across different susceptibility zones. The LDI is calculated by overlaying the landslide inventory on the susceptibility maps and determining the density of landslides within each susceptibility class. Higher landslide densities in high-susceptibility zones indicate better model performance. For the FR model, the LDI values ranged from 0.75 in low-susceptibility zones to 1.80 in extremely high-susceptibility zones. For the IV model, the LDI values ranged from zero in low-susceptibility zones to 3.20 in extremely high-susceptibility zones. These results indicate that the low landslide susceptibility zones have low or zero LDI values, while the extremely high susceptibility zones have high LDI values. This pattern confirms that both the FR and IV methods are correct and validate the models effectively. By combining ROC/AUC

analysis and LDI evaluation, the validation framework robustly confirmed the accuracy and reliability of the FR and IV models. High AUC values and significant LDI values in predicted high-susceptibility zones underscored the models' effectiveness. These validated models are crucial for effective disaster risk management and land-use planning, aiding in the identification of vulnerable zones and guiding mitigation efforts. (refer Table 3 for LDI calculation details).

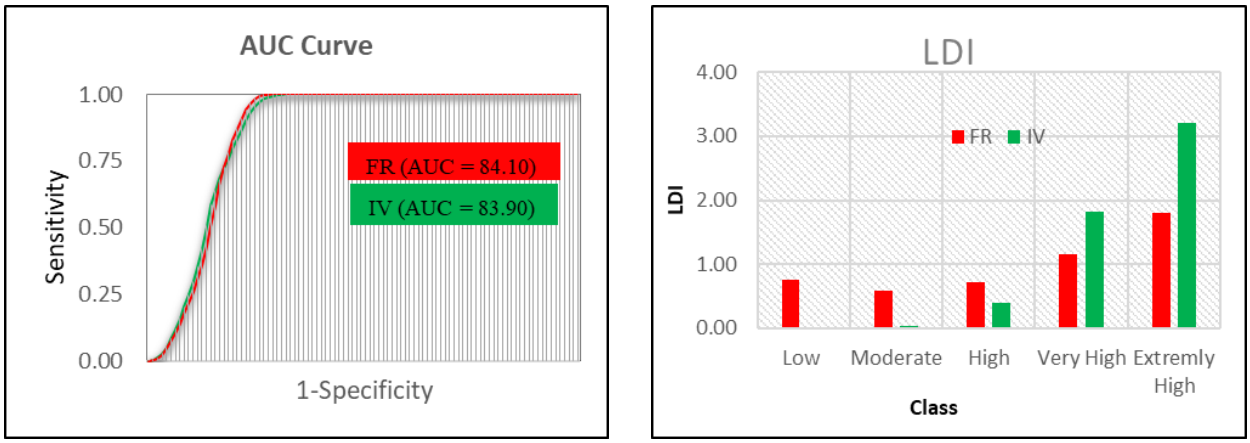


(a) (b)

**Figure 11. Validation Chart of a) AUC Curve and b) LDI Index of different susceptibility class charts.**

**Table 3. LDI index for Landslide susceptibility maps of FR and IV model**

| Model | Class | LSI_Pix | LS_T_Pix | LSI_Pix % | LS_T_Pix% | LDI Class |
|---|---|---|---|---|---|---|
| FR | Low | 474018 | 53 | 5.91% | 4.42% | 0.75 |
| | Moderate | 1368344 | 121 | 17.06% | 10.09% | 0.59 |
| | High | 2530896 | 270 | 31.55% | 22.52% | 0.71 |
| | Very High | 2366498 | 410 | 29.50% | 34.20% | 1.16 |
| | Extreme High | 1281624 | 345 | 15.98% | 28.77% | 1.80 |
| IV | Low | 1087812 | 0 | 13.56% | 0.00% | 0.00 |
| | Moderate | 1655520 | 8 | 20.64% | 0.67% | 0.03 |
| | High | 2195255 | 131 | 27.37% | 10.93% | 0.40 |
| | Very High | 2016248 | 550 | 25.14% | 45.87% | 1.82 |
| | Extreme High | 1066545 | 510 | 13.30% | 42.54% | 3.20 |

## 5. Conclusions

In conclusion, this study has successfully developed and validated landslide susceptibility maps using Frequency Ratio (FR) and Information Value (IV) models within a GIS framework. Both models exhibited strong predictive capabilities, with the FR model demonstrating slightly better performance in this specific dataset and study area, as evidenced by an AUC value of 84.1 compared to 83.9 for the IV model. The classification into five susceptibility categories—Low, Moderate, High, Very High, and Extremely High—was validated using Landslide Density Index (LDI) values, with the FR model showing an LDI value of 1.8 and the IV model showing an LDI value of 3.2, confirming higher landslide densities in the identified high-susceptibility zones.

Future research directions should focus on integrating advanced machine learning techniques such as XGBoost, Random Forest (RF), Naive Bayes (NB), and K-Nearest Neighbors (KNN) to further enhance the reliability and accuracy of landslide susceptibility mapping. The current models, Frequency Ratio (FR) and Information Value (IV), have limitations, particularly their inability to handle complex, non-linear interactions between causative factors. Advanced machine learning techniques are known for their ability to manage these complex interactions and non-linear relationships, potentially improving model performance compared to traditional statistical methods.

Neural Networks (NNs) can significantly enhance predictive capability by learning complex patterns through multiple layers of interconnected neurons, allowing them to model intricate relationships between input features and landslide occurrences. This deep learning approach enables

NNs to capture high-level abstractions and subtle dependencies within the data, which traditional methods might overlook. Support Vector Machines (SVMs) improve predictive accuracy by finding the optimal hyperplane that separates different classes in the feature space. SVMs are particularly effective in high-dimensional spaces and can handle non-linear boundaries through the use of kernel functions. This capability allows SVMs to model complex decision boundaries, capturing intricate patterns in the data that contribute to landslide susceptibility.

Incorporating these advanced algorithms could also facilitate feature selection and optimization, which are crucial for developing robust and transferable landslide susceptibility models. By addressing the limitations of FR and IV models, these techniques can significantly contribute to the improvement of landslide susceptibility mapping, providing more accurate and reliable predictions.

Additionally, exploring the temporal dynamics of landslide susceptibility and incorporating real-time monitoring data would provide valuable insights into the evolving nature of landslide hazards. Developing robust early warning systems based on these advanced models would significantly contribute to proactive disaster risk management and mitigation strategies. Furthermore, future studies should prioritize assessing the transferability and generalizability of the developed landslide susceptibility models to other regions with similar geological and environmental characteristics. This would facilitate broader applications of the models in different geographic contexts, thereby enhancing their utility for land-use planning, infrastructure development, and disaster preparedness at regional and global scales.

## References

[1]. Dhakal, D., Abdi, O., Singh, K., & Sharma, A. (2023). Applications of GIS and Remote Sensing in Highway Project: a Review. *Journal of Mining and Environment (JME), 15 (2),* 1–13.

[2]. Singh, K. & Kumar, V. (2017). Landslide hazard mapping along national highway-154A in Himachal Pradesh, India using information value and frequency ratio. *Arabian Journal of Geosciences, 10 (539),* 1-18.

[3]. Wubalem, A. & Meten, M. (2020). Landslide susceptibility mapping using information value and logistic regression models in Goncha Siso Eneses area, northwestern Ethiopia. *SN Applied Sciences, 2 (807),* 1-19.

[4]. Batar, A.K. & Watanabe, T. (2021). Landslide susceptibility mapping and assessment using geospatial platforms and weights of evidence (WoE) method in the Indian himalayan region: Recent developments, gaps, and future directions. *ISPRS International Journal of Geo-Information, 10 (114),* 1-28.

[5]. Jaiswal, A., Verma, A.K., & Singh, T.N. (2023). Evaluation of slope stability through rock mass classification and kinematic analysis of some major slopes along NH-1A from Ramban to Banihal, North Western Himalayas. *Journal of Rock Mechanics and Geotechnical Engineering, 16,* 167-182.

[6]. Jin, L., Wei, J., Luo, C., & Qin, T. (2023). Slope stability analysis based on improved radial movement optimization considering seepage effect. *Alexandria Engineering Journal, 79,* 591–607.

[7]. Asmare, D. (2023). Application and validation of AHP and FR methods for landslide susceptibility mapping around choke mountain, northwestern ethiopia. *Scientific African, 19*.

[8]. Lima, P., Steger, S., Glade, T., & Mergili, M. (2023). Conventional data-driven landslide susceptibility models may only tell us half of the story: Potential underestimation of landslide impact areas depending on the modeling design. *Geomorphology, 430*.

[9]. Wubalem, A. (2023). Modeling of land suitability for surface irrigation using analytical hierarchy process method in Belessa Districts, northwestern Ethiopia. *Heliyon, 9 (3)*.

[10]. Junaid, M., Abdullah, R.A., Abdelrahman, K., Ullah, A., Mahmood, S., Sa'ari, R., et al. (2024). Assigning resistivity values to rock quality designation indices using integrated unmanned aerial vehicle and 2D electrical resistivity tomography in granitic rock. *Geocarto International, 39 (1).*

[11]. Sari, M., Seren, A., & Alemdag, S. (2020). Determination of geological structures by geophysical and geotechnical techniques in Kırklartepe Dam Site (Turkey). *Journal of Applied Geophysics, 182.*

[12]. Rangari, K. & Chaubey Ravi Shankar (2017). Macro scale (1:50,000) landslide susceptibility mapping in parts of Kullu, Mandi, Chamba, Kangra and Lahaul & Spiti districts of Himachal Pradesh. *Journal of Engineering Geology, XLII (1,2),* 224–233.

[13]. Agrawal, N. & Dixit, J. (2023). GIS-based landslide susceptibility mapping of the Meghalaya-Shillong Plateau region using machine learning algorithms. *Bulletin of Engineering Geology and the Environment, 82 (5).*

[14]. Singh, K. & Kumar, V. (2021). Slope stability analysis of landslide zones in the part of Himalaya, Chamba, Himachal Pradesh, India. *Environmental Earth Sciences, 80 (8).*

[15]. Pachuau, L. (2019). Zonation of Landslide Susceptibility and Risk Assessment in Serchhip town, Mizoram. *Journal of the Indian Society of Remote Sensing, 47 (9),* 1587–1597.

[16]. Singh, K. & Kumar, V. (2018). Hazard assessment of landslide disaster using information value method and analytical hierarchy process in highly tectonic Chamba region in bosom of Himalaya. *Journal of Mountain Science, 15 (4),* 808–824.

[17]. Singh, K. & Kumar, V. (2018). Hazard assessment of landslide disaster using information value method and analytical hierarchy process in highly tectonic Chamba region in bosom of Himalaya. *Journal of Mountain Science, 15 (4),* 808–824.

[18]. Banerjee, P., Ghose, M.K., & Pradhan, R. (2018). Analytic hierarchy process and information value method-based landslide susceptibility mapping and vehicle vulnerability assessment along a highway in Sikkim Himalaya. *Arabian Journal of Geosciences, 11 (7).*

[19]. Es-smairi, A., Elmoutchou, B., Mir, R.A., Ouazani Touhami, A. El, & Namous, M. (2023). Delineation of landslide susceptible zones using Frequency Ratio (FR) and Shannon Entropy (SE) models in northern Rif, Morocco. *Geosystems and Geoenvironment, 2 (4).*

[20]. Veerappan, R., Negi, A., & Siddan, A. (2017). Landslide Susceptibility Mapping and Comparison Using Frequency Ratio and Analytical Hierarchy Process in Part of NH-58, Uttarakhand, India. in: Advancing Culture of Living with Landslides, *Springer International Publishing,* 1081–1091.

[21]. Ramesh, V. & Anbazhagan, S. (2015). Landslide susceptibility mapping along Kolli hills Ghat road section (India) using frequency ratio, relative effect and fuzzy logic models. *Environmental Earth Sciences, 73 (12),* 8009–8021.

[22]. Sangeeta & Maheshwari, B.K. (2019). Earthquake-Induced Landslide Hazard Assessment of Chamoli District, Uttarakhand Using Relative Frequency Ratio Method. *Indian Geotechnical Journal, 49 (1),* 108–123.

[23]. Agrawal, N. & Dixit, J. (2023). GIS-based landslide susceptibility mapping of the Meghalaya-Shillong Plateau region using machine learning algorithms. *Bulletin of Engineering Geology and the Environment, 82 (5).*

[24]. Bhargava, O.N. (2008). An updated introduction to the Spiti geology. *Journal of the Palaeontological Society of India, 53(2),* 113-129

[25]. Arvind Bhardwaj, S., Rai, I., Rana, P., SSRandhawa, A., & Bhardwaj, A. (2014). A Technical Report on the Lake Formation along Billing Lungpa, Lahaul & Spiti District Himachal Pradesh Type of Report Scientific Report. *H.P. State Center on Climate Change (State Council for Science Technology & Environment), 34 SDA Complex, Kasumpti, Shimla-9, Himachal Pradesh, India.*

[26]. Tomás, R., Delgado, J., and Serón, J.B. (2007). Modification of Slope Mass Rating (SMR) by continuous functions. *International Journal of Rock Mechanics and Mining Sciences, 44*, 1062-1069.

[27]. Patidar, A.K., Maurya, D.M., Thakkar, M.G., & Chamyal, L.S. (2007). Fluvial geomorphology and neotectonic activity based on field and GPR data, Katrol hill range, Kachchh, Western India. *Quaternary International, 159 (1),* 74–92.

[28]. Kour, J., Balgotra, S., Rajput, P., Kour, H., Verma, P.K., & Sawant, S.D. (2020). Medicinal Value of High-Altitude Plants of Indian Himalaya. Botanical Leads for Drug Discovery, *Springer Singapore, Singapore,* 295–324.

[29]. Hammer, M. (2010). Mountain ghosts: snow leopards and other animals in the mountains of the Altai Republic, Central Asia. *Biosphere Expeditions*.

[30]. Mishra, A.K. (2023). Tabo Monastery (996 CE) A Vernacular Architecture of Lahaul and Spiti Region of Himachal Pradesh, India: A Preliminary Investigation of Deterioration and Conservation of Murals of gSer-Khang Gumpha. Nakhara: *Journal of Environmental Design and Planning. 22 (1).*

[31]. Killeen, J., Jaupi, L., and Barrett, B. (2022). Impact assessment of humanitarian demining using object-based peri-urban land cover classification and morphological building detection from VHR Worldview imagery. *Remote Sensing Applications: Society and Environment, 27.*

[32]. Shano, L., Raghuvanshi, T.K., & Meten, M. (2020). Landslide susceptibility evaluation and hazard zonation techniques – a review. *Geoenvironmental Disasters, 7 (1).*

[33]. Feizizadeh, B., Jankowski, P., & Blaschke, T. (2014). A GIS based spatially-explicit sensitivity and uncertainty analysis approach for multi-criteria decision analysis. *Computers and Geosciences, 64,* 81–95.

[34]. Anusha, B.N., Babu, K.R., Kumar, B.P., Sree, P.P., Veeraswamy, G., Swarnapriya, C., et al. (2023). Integrated studies for land suitability analysis towards sustainable agricultural development in semi-arid regions of AP, India. *Geosystems and Geoenvironment, 2 (2).*

[35]. Zeng, T., Wu, L., Peduto, D., Glade, T., Hayakawa, Y.S., & Yin, K. (2023). Ensemble learning framework for landslide susceptibility mapping: Different basic classifier and ensemble strategy. *Geoscience Frontiers, 14 (6).*

[36]. Zhou, X., Wen, H., Zhang, Y., Xu, J., & Zhang, W. (2021). Landslide susceptibility mapping using hybrid random forest with Geo detector and RFE for factor optimization. *Geoscience Frontiers, 12 (5).*

[37]. Kamal, A.S.M.M., Ahmed, B., Tasnim, S., & Sammonds, P. (2022). Assessing rainfall-induced landslide risk in a humanitarian context: The Kutupalong Rohingya Camp in Cox's Bazar, Bangladesh. *Natural Hazards Research, 2 (3),* 230–248.

[38]. He, Y., Zhao, Z., Yang, W., Yan, H., Wang, W., Yao, S., et al. (2021). A unified network of information considering superimposed landslide factors sequence and pixel spatial neighborhood for landslide susceptibility mapping. *International Journal of Applied Earth Observation and Geoinformation, 104.*

[39]. Swain, J.B., Singh, N.J., and Gupta, L.R. (2023). Landslide susceptibility zonation of a hilly region: A quantitative approach. *Natural Hazards Research, 4,* 75-86.

[40]. Sweta, K., Goswami, A., Peethambaran, B., Bahuguna, I.M., & Rajawat, A.S. (2022). Landslide susceptibility zonation around Dharamshala, Himachal Pradesh, India: an artificial intelligence model–based assessment. *Bulletin of Engineering Geology and the Environment, 81 (8).*

[41]. Lallianthanga, R.K. & Lalbiakmawia, F. (2014). Landslide Susceptibility Zonation of Kolasib District, Mizoram, India Using Remote Sensing and GIS Techniques. *C)International Journal of Engineering Sciences & Research Technology, 3 (3).*

[42]. Chaturvedi, P., Srivastava, S., & Kaur, P.B. (2017). Landslide early warning system development using statistical analysis of sensors' data at tangni landslide, Uttarakhand, India. *Advances in Intelligent Systems and Computing, Springer Verlag,* 259–270.

[43]. Xu, C. (2015). Preparation of earthquake-triggered landslide inventory maps using remote sensing and GIS technologies: Principles and case studies. *Geoscience Frontiers, 6 (6),* 825–836.

[44]. Lallianthanga, R.K., Lalbiakmawia, F., and Lalramchuana, F. (2013). Landslide Hazard Zonation of Mamit Town, Mizoram, India using Remote Sensing and GIS Techniques. *International Journal of Geology, Earth and Environmental Sciences, 3(1),* 184-194

[45]. Verma, R. (2014). Landslide Hazard in Mizoram: Case Study of Laipuitlang Landslide, Aizawl. *International Journal of Science and Research (IJSR), 3(6),* 2262-2266

[46]. Laltanpuia, Z.D. and Lallianthanga, R.K. (2013). Landslide Hazard Zonation of Lunglei Town, Mizoram, India Using High Resolution Satellite Data. *International Journal of Advanced Remote Sensing and GIS, 2(1),* 148-159

[47]. Anbalagan, R., Chakraborty, D., and Kohli, A. (2008). Landslide hazard zonation (LHZ) mapping on meso-scale for systematic town planning in mountainous terrain. *Journal of Scientific & Industrial Research, 67,* 486-497

[48]. Lin, M.L. and Tung, C.C. (2004). A GIS-based potential analysis of the landslides induced by the Chi-Chi earthquake. *Engineering Geology. 71 (1–2),* 63–77.

[49]. Herold, M., Latham, J.S., Di Gregorio, A., and Schmullius, C.C. (2006). Evolving standards in land cover characterization. *Journal of Land Use Science, 1 (2–4),* 157–168.

[50]. Kumar, R. & Anbalagan, R. (2016). Landslide Susceptibility Mapping Using Analytical Hierarchy Process (AHP) in Tehri Reservoir Rim Region, Uttarakhand. *Journal Geological Society of India, 87,* 271-286.

[51]. Gadtaula, A. & Dhakal, S. (2019). Landslide susceptibility mapping using Weight of Evidence Method in Haku, Rasuwa District, Nepal. *Journal of Nepal Geological Society, 58,* 163–171.

[52]. Badola, S., Mishra, V.N., Parkash, S., & Pandey, M. (2023). Rule-based fuzzy inference system for landslide susceptibility mapping along national highway 7 in Garhwal Himalayas, India. *Quaternary Science Advances, 11,* 100093.

[53]. R M, Y. & Dolui, B. (2021). Statistical and machine intelligence based model for landslide susceptibility mapping of Nilgiri district in India. *Environmental Challenges, 5.*

[54]. Xu, H., He, X., Pradhan, B., & Sheng, D. (2023). A pre-trained deep-learning surrogate model for slope stability analysis with spatial variability. *Soils and Foundations, 63 (3).*

[55]. Deng, D. ping, Li, L., & Zhao, L. heng (2017). Limit equilibrium method (LEM) of slope stability and calculation of comprehensive factor of safety with double strength-reduction technique. *Journal of Mountain Science, 14 (11),* 2311–2324.

[56]. Z. T. Bieniawski (1989). Engineering Rock Mass Classifications_ A Complete Manual for Engineers and Geologists in Mining, Civil, and Petroleum Engineering. *A Wiley-Inter science Publication, Canada.*

[57]. Tiwari, B., Asce, M., & Do, H. (2011). Deterministic Seismic Hazard Analysis of a Highway Sector with GIS. *Geo-Frontiers © ASCE 2011,* 1554–1563.

[58]. Joshi, J., Bharadwaj, D., Paudyal, P., & Timalsina, N. (2017). Landslide inventory, susceptibility mapping and recommendation of the mitigation measures in Nuwakot district. *Journal of Nepal Geological Society, 53,* 107–118.

[59]. Huang, F., Teng, Z., Guo, Z., Catani, F., & Huang, J. (2023). Uncertainties of landslide susceptibility prediction: Influences of different spatial resolutions, machine learning models and proportions of training and testing dataset. *Rock Mechanics Bulletin, 2 (1),* 100028.

[60]. Ciampalini, A., Raspini, F., Bianchini, S., Frodella, W., Bardi, F., Lagomarsino, D., et al. (2015). Remote sensing as tool for development of landslide databases: The case of the Messina Province (Italy) geodatabase. *Geomorphology, 249,* 103–118.

[61]. Shao, X. & Xu, C. (2022). Earthquake-induced landslides susceptibility assessment: A review of the state-of-the-art. *Natural Hazards Research, 2 (3),* 172–182.

[62]. Dahal, R.K., Hasegawa, S., Nonomura, A., Yamanaka, M., Masuda, T., & Nishino, K. (2008). GIS-based weights-of-evidence modelling of rainfall-induced landslides in small catchments for landslide susceptibility mapping. *Environmental Geology, 54 (2),* 311–324.

[63]. Nagarajan, R. (2002). Rapid assessment procedure to demarcate areas susceptible to earthquake-induced ground failures for environment management - A case study from parts of northeast India. *Bulletin of Engineering Geology and the Environment, 61 (2),* 99–119.

[64]. Nandy, S., Singh, C., Das, K.K., Kingma, N.C., & Kushwaha, S.P.S. (2015). Environmental vulnerability assessment of eco-development zone of Great Himalayan National Park, Himachal Pradesh, India. *Ecological Indicators, 57,* 182–195.

[65]. Chen, C.Y. & Huang, W.L. (2013). Land use change and landslide characteristics analysis for community-based disaster mitigation. *Environmental Monitoring and Assessment, 185 (5),* 4125–4139.

[66]. Frattini, P., Crosta, G., & Carrara, A. (2010). Techniques for evaluating the performance of landslide susceptibility models. *Engineering Geology, 111 (1–4),* 62–72.

[67]. Ikram, Q.D., Jamalzi, A.R., Hamidi, A.R., Ullah, I., & Shahab, M. (2024). Flood risk assessment of the population in Afghanistan: A spatial analysis of hazard, exposure, and vulnerability. *Natural Hazards Research, 4 (1),* 46–55.

[68]. Thi Ngo, P.T., Panahi, M., Khosravi, K., Ghorbanzadeh, O., Kariminejad, N., Cerda, A., et al. (2021). Evaluation of deep learning algorithms for national scale landslide susceptibility mapping of Iran. *Geoscience Frontiers, 12 (2),* 505–519.

[69]. Tyagi, A., Kamal Tiwari, R., & James, N. (2022). A review on spatial, temporal and magnitude prediction of landslide hazard. *Journal of Asian Earth Sciences: X. 7.*

[70]. Cook, M.E., Brook, M.S., Hamling, I.J., Cave, M., Tunnicliffe, J.F., & Holley, R. (2023). Investigating slow-moving shallow soil landslides using Sentinel-1 InSAR data in Gisborne, New Zealand. *Landslides, 20 (2),* 427–446.

[71]. Tempa, K., Peljor, K., Wangdi, S., Ghalley, R., Jamtsho, K., Ghalley, S., et al. (2021). UAV technique to localize landslide susceptibility and mitigation proposal: A case of Rinchending Goenpa landslide in Bhutan. *Natural Hazards Research. 1 (4),* 171–186.

[72]. Huang, F., Yan, J., Fan, X., Yao, C., Huang, J., Chen, W., et al. (2022). Uncertainty pattern in landslide susceptibility prediction modelling: Effects of different landslide boundaries and spatial shape expressions. *Geoscience Frontiers, 13 (2).*

[73]. Chowdhury, M.S. (2023). A review on landslide susceptibility mapping research in Bangladesh. *Heliyon, 9 (7).*

[74]. Hammad Khaliq, A., Basharat, M., Talha Riaz, M., Tayyib Riaz, M., Wani, S., Al-Ansari, N., et al. (2023). Spatiotemporal landslide susceptibility mapping using machine learning models: A case study from district Hattian Bala, NW Himalaya, Pakistan. *Ain Shams Engineering Journal, 14 (3).*

[75]. Panchal, S. & Shrivastava, A.K. (2022). Landslide hazard assessment using analytic hierarchy process (AHP): A case study of National Highway 5 in India. *Ain Shams Engineering Journal, 13 (3).*

[76]. Khan, A.I. & Al-Mulla, Y. (2019). Unmanned aerial vehicle in the machine learning environment. *Procedia Comput Sci, Elsevier B.V.,* 46–53.

[77]. Mandal, K., Saha, S., & Mandal, S. (2021). Applying deep learning and benchmark machine learning algorithms for landslide susceptibility modelling in Rorachu river basin of Sikkim Himalaya, India. *Geoscience Frontiers, 12 (5).*

[78]. Hong, H. (2023). Assessing landslide susceptibility based on hybrid Best-first decision tree with ensemble learning model. *Ecological Indicators, 147.*

[79]. Gautam, D., Neupane, P., & Raj Paudyal, K. (2018). Landslide inventory mapping and assessment along the Ramche-Jharlang area in Dhading, Rasuwa and Nuwakot districts, Lesser Himalaya Central Nepal. *Journal of Nepal Geological Society, 55 (Sp. Issue),* 103–108

[80]. Feizizadeh, B., Shadman Roodposhti, M., Jankowski, P., & Blaschke, T. (2014). A GIS-based extended fuzzy multi-criteria evaluation for landslide susceptibility mapping. *Computers and Geosciences. 73,* 208–221.

[81]. Ali, S.A., Parvin, F., Vojteková, J., Costache, R., Linh, N.T.T., Pham, Q.B., et al. (2021). GIS-based landslide susceptibility modeling: A comparison between fuzzy multi-criteria and machine learning algorithms. *Geoscience Frontiers, 12 (2),* 857–876.

[82]. Achour, Y. & Pourghasemi, H.R. (2020). How do machine learning techniques help in increasing accuracy of landslide susceptibility maps? *Geoscience Frontiers, 11 (3),* 871–883.

[83]. Saha, S., Majumdar, P., & Bera, B. (2023). Deep learning and benchmark machine learning based landslide susceptibility investigation, Garhwal Himalaya (India). *Quaternary Science Advances, 10*.

[84]. Das, J., Saha, P., Mitra, R., Alam, A., & Kamruzzaman, M. (2023). GIS-based data-driven bivariate statistical models for landslide susceptibility prediction in Upper Tista Basin, India. *Heliyon, 9 (5).*

[85]. Ullah, K., Wang, Y., Fang, Z., Wang, L., & Rahman, M. (2022). Multi-hazard susceptibility mapping based on Convolutional Neural Networks. *Geoscience Frontiers, 13 (5).*

[86]. Paryani, S., Neshat, A., & Pradhan, B. (2021). Improvement of landslide spatial modeling using machine learning methods and two Harris hawks and bat algorithms. *Egyptian Journal of Remote Sensing and Space Science, 24 (3),* 845–855.

[87]. Muñoz-Torrero Manchado, A., Antonio Ballesteros-Cánovas, J., Allen, S., & Stoffel, M. (2022). Deforestation controls landside susceptibility in Far-Western Nepal. *Catena, 219.*

[88]. Grabowski, D., Laskowicz, I., Małka, A., & Rubinkiewicz, J. (2022). Geoenvironmental conditioning of landsliding in river valleys of lowland regions and its significance in landslide susceptibility assessment: A case study in the Lower Vistula Valley, Northern Poland. *Geomorphology, 419.*

[89]. Kamran, M. & Yamamoto, K. (2023). Evolution and use of remote sensing in ecological vulnerability assessment: A review. *Ecological Indicators, 148.*

[90]. Tangdamrongsub, N., Han, S.C., Jasinski, M.F., & Šprlák, M. (2019). Quantifying water storage change and land subsidence induced by reservoir impoundment using GRACE, Landsat, and GPS data. *Remote Sensing of Environment, 233.*

[91]. Chang, Z., Catani, F., Huang, F., Liu, G., Meena, S.R., Huang, J., et al. (2023). Landslide susceptibility prediction using slope unit-based machine learning models considering the heterogeneity of conditioning factors. *Journal of Rock Mechanics and Geotechnical Engineering, 15 (5),* 1127–1143.

[92]. Dhungana, G., Ghimire, R., Poudel, R., & Kumal, S. (2023). Landslide susceptibility and risk analysis in Benighat Rural Municipality, Dhading, Nepal. *Natural Hazards Research, 3 (2),* 170–185.

[93]. Patil, A.S. & Panhalkar, S.S. (2023). Remote sensing and GIS-based landslide susceptibility mapping using LNRF method in part of Western Ghats of India. *Quaternary Science Advances, 11,* 100095.

[94]. Ciampalini, A., Raspini, F., Lagomarsino, D., Catani, F., & Casagli, N. (2016). Landslide susceptibility map refinement using PSInSAR data. *Remote Sensing of Environment, 184,* 302–315.

[95]. Roy, J. & Saha, S. (2022). Ensemble hybrid machine learning methods for gully erosion susceptibility mapping: K-fold cross validation approach. *Artificial Intelligence in Geosciences, 3,* 28–45.

[96]. Wei, R., Ye, C., Sui, T., Ge, Y., Li, Y., & Li, J. (2022). Combining spatial response features and machine learning classifiers for landslide susceptibility mapping. *International Journal of Applied Earth Observation and Geoinformation, 107.*

[97]. Youssef, A.M. & Pourghasemi, H.R. (2021). Landslide susceptibility mapping using machine learning algorithms and comparison of their performance at Abha Basin, Asir Region, Saudi Arabia. *Geoscience Frontiers, 12 (2),* 639–655.

[98]. Saha, A. & Saha, S. (2022). Integrating the artificial intelligence and hybrid machine learning algorithms for improving the accuracy of spatial prediction of landslide hazards in Kurseong Himalayan Region. *Artificial Intelligence in Geosciences, 3,* 14–27.

[99]. Nandi, A. & Shakoor, A. (2010). A GIS-based landslide susceptibility evaluation using bivariate and multivariate statistical analyses. *Engineering Geology, 110 (1–2),* 11–20.

# یک رویکرد جغرافیایی به نقشه‌برداری حساسیت زمین لغزش اسپیتی، هند

**دوراج داکال* و کانوارپریت سینگ**

**گروه مهندسی عمران، دانشگاه چاندیگرا، موهالی، هند**

ارسال ۲۰۲۴/۰۶/۱۹، پذیرش ۲۰۲۴/۰۸/۱۰

* نویسنده مسئول مکاتبات: fewdrd@gmail.com

**چکیده:**

زمین لغزش خطرات قابل توجهی برای زندگی انسان، زیرساخت‌ها و محیط زیست به ویژه در مناطق ناپایدار زمین شناسی مانند هیمالیا ایجاد می‌کند. هدف این مطالعه توسعه و اعتبار سنجی نقشه‌های حساسیت زمین لغزش با استفاده از مدل‌های نسبت فراوانی (FR) و ارزش اطلاعات (IV) در چارچوب GIS است. استفاده از داده‌های مکانی با وضوح بالا، از جمله عوامل ژئومورفولوژیکی، توپوگرافی، و هیدرولوژیکی به دست آمده از مدل‌های ارتفاعی دیجیتال با وضوح بالا (DEMs) و سایر مجموعه‌های داده‌های مکانی. نقشه‌های حساسیت به پنج دسته کم، متوسط، زیاد، بسیار زیاد و بسیار زیاد طبقه بندی شدند. مدل‌ها با استفاده از فهرست زمین لغزش ۱۳۱۳ رویداد زمین لغزش، با تقسیم ۷۰:۳۰ برای آموزش و آزمایش مجموعه داده‌ها آموزش و اعتبارسنجی شدند. عملکرد پیش‌بینی‌کننده مدل‌ها با استفاده از ناحیه زیر منحنی (AUC) منحنی مشخصه عملیاتی گیرنده (ROC) ارزیابی شد، که مقادیر AUC 84.1 برای مدل FR و ۸۳.۹ برای مدل IV به دست آمد. شاخص تراکم زمین لغزش (LDI) قابلیت اطمینان مدل‌ها را بیشتر تایید کرد، که نشان دهنده تراکم زمین لغزش بالاتر در مناطق با حساسیت بالا پیش بینی شده است. این مطالعه نشان می‌دهد که هر دو مدل FR و IV ابزارهای مؤثری برای نقشه‌برداری حساسیت زمین لغزش و اعتبارسنجی آن هستند. یافته‌ها دقت پیش‌بینی برتر مدل FR را در این زمینه خاص برجسته می‌کنند. تحقیقات آینده باید از تکنیک‌های پیشرفته یادگیری ماشینی مانند XGBoost، Random Forest (RF)، Naive Bayes (NB) و K-Nearest Neighbors (KNN) برای افزایش قابلیت اطمینان و دقت مدل‌های حساسیت زمین لغزش استفاده کند.

**کلمات کلیدی:** نگاشت حساسیت به زمین لغزش (LSM)، نسبت فرکانس (FR)، ارزش اطلاعات (IV)، تحلیل مکانی، شاخص تراکم زمین لغزش (LDI).